

Warped 5-Dimensional Models: Phenomenological Status and Experimental Prospects

Hooman Davoudiasl

E-mail: hooman@bnl.gov

Department of Physics, Brookhaven National Laboratory, Upton, NY 11973-5000,
USA

Shrihari Gopalakrishna

E-mail: shri@quark.phy.bnl.gov

Department of Physics, Brookhaven National Laboratory, Upton, NY 11973-5000,
USA

Eduardo Pontón

E-mail: eponton@phys.columbia.edu

Department of Physics, Columbia University, 538 W. 120th St, New York, NY 10027,
USA

José Santiago

E-mail: santiago@itp.phys.ethz.ch

Institute for Theoretical Physics, ETH, CH-8093, Zürich, Switzerland

Abstract.

Warped 5-dimensional models, based on the original Randall-Sundrum geometry, have been extended beyond their initial purpose of resolving the gauge hierarchy problem. Over the past decade, various ingredients have been added to their basic structure in order to provide natural and predictive models of flavor and also to address existing constraints from precision data. In this review, we examine the theoretical and experimental status of realistic models that accommodate current data, while addressing the hierarchy and flavor puzzles of the Standard Model. We also discuss the prospects for future discovery of the TeV-scale Kaluza-Klein states that are predicted to emerge in these models, and outline some of the challenges that the detection of such particles pose for experiments at the Large Hadron Collider.

1. Introduction

The Standard Model (SM) of particle physics is remarkably successful in explaining a wide range of microscopic phenomena and has passed numerous tests over the past few decades. The only ingredient of this model that has yet to be discovered is the Higgs boson. It is the vacuum expectation value (vev) of this field that breaks the electroweak (EW) symmetry $SU(2)_L \times U(1)_Y$ down to $U(1)_{EM}$ of quantum electrodynamics and provides masses for elementary particles in the SM. However, this picture, though economical, leaves some intriguing questions unanswered. One obvious and central question is related to the patterns of the SM fermion masses (that, including the neutrinos, span 12 orders of magnitude!) and mixing; this is the *flavor puzzle* and is based on firm experimental evidence.

Another question, which is more theoretical in nature, arises when one considers the effect of quantum corrections on the Higgs vev. These corrections are quadratically sensitive to any physical mass scales that could emerge at energies above the weak scale $M_W \sim 100$ GeV. However, stringent requirements from precision data strongly suggest that new physics can only appear at scales much larger than M_W . Besides, very high physical scales are well-motivated in the context of a Grand Unified Theory (GUT) or theories of quantum gravity. Therefore, one is faced with the question of what stabilizes the Higgs potential well below such large scales. The severest version of this problem arises when the fundamental cutoff scale is assumed to be near the 4D Planck mass $M_P \sim 10^{19}$ GeV; this is the *hierarchy problem*.

In this review, we will focus on a framework based on a model originally proposed by Randall and Sundrum [1] to address the hierarchy problem. The Randall-Sundrum (RS) model is based on a slice of AdS_5 spacetime between two flat 4D boundaries, often referred to as the UV (Planck) and IR (TeV) branes. The branes are assumed to be separated by a distance of order the curvature radius of the background, which is in turn of order the 5D fundamental scale M_5 . This model provides a natural resolution of the hierarchy, by exponentially generating the weak scale from scales of order $M_5 \sim M_P$. To achieve this, the Higgs field is localized at the IR-brane and the warping along the fifth dimension redshifts the Planckian 5D Higgs vev down to the weak scale. The requisite brane separation was shown to be easily obtained in simple models [2], resulting in a stable geometry.

In the original RS model all SM fields were localized on the IR-brane and the most distinct signature of this setup was the emergence of a spin-2 tower of Kaluza-Klein (KK) gravitons [3] at the TeV scale. However, it was soon realized that resolving the hierarchy only required the Higgs to be IR-localized [4] and other fields could propagate in the 5D bulk. The SM gauge sector [5, 6] and the fermions [7] were then promoted to 5D fields. It was shown that localization of fermion zero modes could be achieved using 5D mass terms [7], with the heavy fermions localized toward the Higgs and the light fields localized away from the Higgs, resulting in a natural and predictive model of flavor. In particular, given that 5D location sets the relevant physical mass scale in the

RS background, light-flavor 4-fermion operators are governed by large cutoff scales in warped flavor models [8], as required by precision data. This interesting feature allows one to address both the hierarchy and flavor puzzles within RS-type models, making them a very attractive model building framework that can be experimentally tested at the weak scale.

While warped 5D models explain some of the important unresolved issues of the SM to a large extent, they are still subject to a degree of (fine-)tuning, once confronted with precision EW [9] and flavor data [10]-[14]. The gist of this tension is traced back to the resolution of the hierarchy problem that would prefer the scale of new physics to be near M_W . This gives rise to an effective 4D cutoff scale in the TeV range, where all non-renormalizable interactions that are not forbidden by a symmetry will emerge, whereas precision data generally require the cutoff scale to be at $\mathcal{O}(10)$ TeV or more. To eliminate such “little hierarchies,” the basic 5D SM structure of warped models have been augmented by various new ingredients, such as larger gauge symmetry groups [15, 16], in order to keep the scale of KK modes in the few-TeV range. This would remove the need for inordinate amounts of (fine-)tuning and also make the models more likely to be testable in various high energy experiments.

Even though the most recent warped models of hierarchy and flavor can accommodate KK masses as low as 2-3 TeV [9], the discovery of the signature states quite generically poses a significant challenge. The basic reason for this originates in the way various states are localized in the bulk: light fermions are UV-localized, whereas the KK modes and heavy fermions are IR-localized. This suppresses the couplings of the KK modes to light flavors that are important initial (such as light quarks) and final (such as μ^\pm) states in collider production and detection, respectively. A volume suppression also affects the couplings of the highly localized KK modes to gauge fields that are spread over the bulk. Hence, in models that explain the flavor problem we end up with suppressed production of KK modes that eventually decay into heavy fields, such as $t\bar{t}$, requiring complicated event reconstructions. Also, the heavy final states are highly boosted due to the high mass of the KK parent. This makes the eventual decays of the heavy final states into di-jets difficult to distinguish from mono-jets, hence rendering QCD background suppression challenging.

In the first half of this review, we will discuss the theoretical techniques that have been used to analyze the phenomenology of RS-type models. Although our results are of more general applicability, we focus on the most recent prototypical models that incorporate a realistic flavor structure (bulk SM gauge and fermion fields) and possibly allow for new physics within reach of the Large Hadron Collider (LHC). We restrict ourselves to the original RS background and assume that there is a Higgs degree of freedom in the low-energy theory. We survey the phenomenological status of these realistic scenarios, thus providing a guide as to the plausible values of parameters in viable models. Having determined the phenomenologically relevant range of parameters, we will discuss the key collider signatures of warped 5D models in the second half of the review. Our main focus will be models endowed with bulk symmetries that allow for the

KK masses to be within the reach of the LHC, without the need for unnatural choices of parameters. Some of the experimental obstacles that these models pose, as well as proposals to overcome such problems, will be outlined. We will also briefly discuss the expected enhancement of clean signals in “truncated” warped models whose UV cutoff is well below M_P , but still explain flavor. We will conclude with a summary.

Before closing this introduction, we would like to emphasize that this review is not meant to be exhaustive or comprehensive. Such an undertaking will require a much longer article due to the large amount of research performed on warped models, over the past several years. As such, we have limited our survey to some of the most generic features of model building and phenomenology. To the extent possible, we have cited works that are directly or closely related to our discussions. However, unfortunately, many worthy papers have been left out in our review. We hope that this article will serve to present a sufficiently inclusive account of the status of warped models to motivate the interested reader to pursue further references and delve more deeply into some of the subjects that we have (not) considered here.

Part I General Tools and Electroweak Constraints

Contributed by E. Pontón and J. Santiago

In the first part of this review, we describe the tools that have been used to study the physics of warped extra-dimensional scenarios. We have put special emphasis on the explanation and comparison of the different techniques used. We focus on models that incorporate a custodial symmetry, and analyze the constraints from EW precision measurements. There are also important constraints from flavour data that, under the assumption of strict “anarchy” (that the 5D flavor couplings present no structure at all and are all of the same order, including complex phases), can result in rather severe bounds on the new physics. These constraints depend on parameters different from those relevant for the EW precision constraints and can be evaded without significantly modifying the latter. Due to space constraints, we focus on the EW analysis, except for a brief section on flavour where we collect some of the recent references.

2. Methods in models with warped extra dimensions

We consider a 5D space-time with a warped metric, written in conformally flat coordinates as \ddagger

$$ds^2 = a(z)^2(\eta_{\mu\nu}dx^\mu dx^\nu - dz^2) , \quad a(z) = \frac{L_0}{z} , \quad (1)$$

\ddagger Another commonly used form for the AdS metric is $ds^2 = e^{-2ky}\eta_{\mu\nu}dx^\mu dx^\nu - dy^2$, where $k = 1/L_0$ is the AdS curvature. The formulas in conformal coordinates can be transcribed into the “proper distance” coordinates by setting $z/L_0 = e^{ky}$, $\partial_y = a(z)^{-1}\partial_z$ and $dy = a(z)dz$.

where $L_0 \leq z \leq L_1$. Solving the hierarchy problem requires $L_0 \approx M_P^{-1}$, and $L_1 \approx (\text{TeV})^{-1}$, although other choices of scales have proved useful in addressing e.g. the flavour problem [17].

2.1. Kaluza-Klein expansions

We start by collecting the main results for the Kaluza-Klein (KK) wavefunctions associated with spin-2 [3], spin-1 [5, 6] and spin-1/2 [7] fields propagating on the background of Eq. (1) (for a unified derivation, see [8]). The KK wavefunctions are especially useful in studying the collider phenomenology of warped extra dimensions, to be discussed in the second part of this review.

2.1.1. Gauge Bosons The 5D gauge action is

$$S_{\text{gauge}} = -\frac{1}{4g_5^2} \int d^5x \sqrt{g} F_{MN}^a F^{aMN} + S_{\text{gauge}}^{\text{UV}} + S_{\text{gauge}}^{\text{IR}} , \quad (2)$$

where $M, N = 0, 1, 2, 3, z$ run over the 5D coordinates, g_5 is the 5D gauge coupling (with mass dimension $-1/2$), F_{MN}^a is the gauge field strength, a is a gauge index, and $S_{\text{gauge}}^{\text{UV}}, S_{\text{gauge}}^{\text{IR}}$ contain possible brane-localized terms for the gauge fields, to be specified shortly. If the gauge field does not satisfy Dirichlet boundary conditions at both branes (see below) we can go to the unitary gauge, $A_5 = 0$ §, in which the KK decomposition reads

$$A_\mu(x, z) = \sum_n A_\mu^n(x) f_n(z) . \quad (3)$$

The KK wavefunctions satisfy $O(m_n, z)f_n(z) = 0$, where m_n are the gauge KK masses and the differential operator in the coordinates of Eq. (1) is

$$O(p, z) = \partial_z a(z) \partial_z + a(z) p^2 . \quad (4)$$

The solutions are written in terms of Bessel functions of the first and second kind, $J_\alpha(x)$ and $Y_\alpha(x)$, for which we shall use the shorthand notation

$$J_\alpha^{0,1,z} \equiv J_\alpha(m_n L_0), J_\alpha(m_n L_1), J_\alpha(m_n z) , \quad (5)$$

and similarly for $Y_\alpha^{0,1,z}$. Then

$$f_n(z) = A_n a(z)^{-1} [J_1^z + B_n Y_1^z] , \quad (6)$$

where the overall constants A_n are determined by the orthonormality condition

$$\int_{L_0}^{L_1} dz a(z) f_n(z) f_m(z) = L \delta_{mn} , \quad (7)$$

and we defined the volume factor

$$L \equiv \int_{L_0}^{L_1} dz a(z) = L_0 \log \frac{L_1}{L_0} . \quad (8)$$

§ Other gauge choices can also be useful [18]. A gauge independent expansion can be obtained by choosing the KK modes of A_5 equal to $\partial_z f_n / m_n$.

The boundary conditions (b.c.'s) take the form

$$[L_0 \partial_z - a(z) b_{\text{UV}}] f_n(z) \Big|_{z=L_0} = 0 , \quad (9)$$

$$[L_0 \partial_z + a(z) b_{\text{IR}}] f_n(z) \Big|_{z=L_1} = 0 , \quad (10)$$

where the b_i depend on the brane localized terms. For instance, in the presence of localized kinetic terms with coefficients r_i and localized mass terms m_i :

$$b_{\text{UV,IR}} \equiv a_{0,1}^{-2} \hat{r}_{\text{UV,IR}} \hat{m}_n^2 - \hat{m}_{\text{UV,IR}} , \quad (11)$$

where $a_0 \equiv a(L_0)$, $a_1 \equiv a(L_1)$, and we defined dimensionless quantities $\hat{m}_n = m_n L_0$, $\hat{r}_i = r_i / L_0$ and $\hat{m}_i = m_i L_0$ for $i = \text{UV, IR}$ (the natural scale of the dimensionful microscopic parameters is expected to be of order L_0). The b.c. on the IR brane determines $B_n = -\tilde{J}_1^{\text{IR}} / \tilde{Y}_1^{\text{IR}}$, where

$$\tilde{J}_\alpha^{\text{UV,IR}} \equiv \hat{m}_n J_{\alpha-1}^{0,1} \pm a_{0,1} b_{\text{UV,IR}} J_\alpha^{0,1} , \quad (12)$$

and an analogous definition for $\tilde{Y}_\alpha^{\text{UV,IR}}$. The b.c. on the UV brane then leads to the eigenvalue equation

$$\tilde{J}_\alpha^{\text{UV}} \tilde{Y}_\alpha^{\text{IR}} - \tilde{Y}_\alpha^{\text{UV}} \tilde{J}_\alpha^{\text{IR}} = 0 , \quad \text{with } \alpha = 1 , \quad (13)$$

which determines the KK masses, m_n .

The case with $\hat{m}_{\text{UV}} = \hat{m}_{\text{IR}} = 0$ leads to a zero mass eigenvalue, $m_0 = 0$, corresponding to an unbroken 4D gauge symmetry. In the SM electroweak sector, an IR localized Higgs field leads to $\hat{m}_{\text{IR}} \neq 0$ and non-zero Z and W^\pm masses. The Higgsless limit [19] corresponds to $\hat{m}_{\text{IR}} \rightarrow \infty$. A case of interest in the models with custodial symmetry to be introduced in Section 3.1 corresponds to Dirichlet boundary conditions on the UV brane, and can be obtained by taking $\hat{m}_{\text{UV}} \rightarrow \infty$. In the following, for simplicity we will assume that the localized kinetic terms are sufficiently small to be neglected. However, it should be remarked that when $\hat{r}_{\text{IR}} > 1$ these can have important phenomenological consequences [20, 21]. If both b.c.'s are Dirichlet, $\hat{m}_{\text{UV,IR}} \rightarrow \infty$, a zero mode for A_5 remains in the spectrum [22]-[25]. This can have interesting consequences for EWSB [26, 27].

2.1.2. Fermions The fermion action is

$$S_{\text{fermion}} = \int d^5x \sqrt{g} \left\{ \frac{i}{2} \bar{\Psi} e_A^M \Gamma^A D_M \Psi - \frac{i}{2} (D_M \Psi)^\dagger \Gamma^0 e_A^M \Gamma^A \Psi - M \bar{\Psi} \Psi \right\} \\ + S_{\text{fermion}}^{\text{UV}} + S_{\text{fermion}}^{\text{IR}} , \quad (14)$$

where $\Gamma^A = (\gamma^\mu, -i\gamma_5)$ are the flat space Dirac gamma matrices in 5D space, D_M is the covariant derivative with respect to the gauge symmetry as well as general coordinate and local Lorentz transformations \parallel , and $S_{\text{fermion}}^{\text{UV}}$, $S_{\text{fermion}}^{\text{IR}}$ contain possible fermion localized terms. It is convenient to express the 5D mass term in units of $1/L_0$ thus

\parallel For a diagonal metric of the form $ds^2 = a(z)^2 \eta_{\mu\nu} dx^\mu dx^\nu + b(z)^2 dz^2$ the spin connection in D_M cancels out in the fermion action, Eq. (14).

defining a dimensionless parameter $c = ML_0$. The KK decomposition for each 4D chirality of the 5D fermion reads ($\gamma_5 \Psi_{L,R} = \mp \Psi_{L,R}$)

$$\Psi_{L,R}(x, z) = \sum_n \psi_{L,R}^n(x) f_{L,R}^n(z) , \quad (15)$$

where $f_L^n(z)$ and $f_R^n(z)$ are related by $O_c f_L^n = m_n f_R^n$, with

$$O_c = \partial_z - z^{-1} (2 - c) , \quad (16)$$

and m_n are the fermion KK masses. The LH profile, $f_L^n(z)$, obeys the second order differential equation $O_{-c} O_c f_L^n = -m_n^2 f_L^n$. Explicitly, the solution for the LH modes reads

$$f_L^n(z) = A_n^f a(z)^{-5/2} \left[J_{c+1/2}^z + B_n^f Y_{c+1/2}^z \right] , \quad (17)$$

where the overall constants A_n^f are determined by the normalization condition Eq. (7) with $f_n(z) \rightarrow L^{1/2} a(z)^{3/2} f_L^n(z)$.

The b.c.'s for both chiralities are not independent but related by the equations of motion. 4D chirality can be generated at the level of zero modes by a choice of b.c.'s that forbid a zero mode for one of the two chiralities. For instance, a LH zero mode is obtained by choosing b.c.'s for $f_L^n(z)$ as in Eqs. (9) and (10) with $b_{UV,IR} \rightarrow \pm(2-c) + b_{UV,IR}^f$, and b_i^f as in Eq. (11) but with $\hat{n}_i = 0$ and r_i denoting the coefficients of possible fermion brane kinetic terms. Neglecting brane kinetic terms, the corresponding LH zero mode wave function is

$$f_L^0(z) = \sqrt{\frac{(1-2c)}{L_0 [(L_1/L_0)^{(1-2c)} - 1]}} \left(\frac{z}{L_0} \right)^{2-c} , \quad (18)$$

which corresponds to a chiral fermion exponentially localized towards the UV (IR) brane for $c > 1/2$ ($c < 1/2$), while the physical profile is flat for $c = 1/2$. The remaining constants for the massive LH modes in Eq. (17) are given by $B_n^f = -\tilde{J}_{c+1/2}^{IR}/\tilde{Y}_{c+1/2}^{IR}$, where $\tilde{J}_{c+1/2}^{IR}$ and $\tilde{Y}_{c+1/2}^{IR}$ are defined in Eq. (12), taking $b_i = b_i^f$. The profiles for the associated RH chiralities, $f_R^n(z)$, are simply obtained from Eq. (17) by the replacement $c + 1/2 \rightarrow c - 1/2$ [but with exactly the same constants A_n^f and B_n^f that appear in $f_L^n(z)$]. The fermion KK masses are determined by Eq. (13) with $\alpha = c + 1/2$.

If instead the zero mode is right-handed, the corresponding profiles are obtained with the replacement $c \rightarrow -c$ everywhere in Eqs. (17) and (18) (and exchanging the LH fields by the RH ones).

2.1.3. Gravitons KK excitations of the graviton (spin-2 resonances) may give a striking signature of the extra-dimensional structure. We summarize briefly the relevant results for the graviton KK wavefunctions. The tensor fluctuations $h_{\mu\nu}$ are introduced by making $\eta_{\mu\nu} \rightarrow \eta_{\mu\nu} + h_{\mu\nu}(x, z)$ in Eq. (1). Starting from the Einstein-Hilbert action, linearizing in $h_{\mu\nu}$, and choosing the transverse-traceless gauge, $\partial^\mu h_{\mu\nu} = h_\alpha^\alpha = 0$, the KK expansion reads

$$h_{\mu\nu}(x, z) = \sum_n h_{\mu\nu}^n(x) f_n^G(z) , \quad (19)$$

where $[a(z)^{-3}\partial_z a^3(z)\partial_z + m_n^2] f_n^G(z) = 0$, so that [see the definitions of Eq. (5)]

$$f_n^G(z) = A_n^G a(z)^{-2} [J_2^z + B_n^G Y_2^z] . \quad (20)$$

The normalization constants A_n^G are obtained from Eq. (7) with $f_n(z) \rightarrow a(z)f_n^G(z)$. Localized curvature (“kinetic”) terms [28] can be introduced through the functions of Eq. (12), as was done for gauge and fermion fields, so that $B_n^G = -\tilde{J}_2^{\text{IR}}/\tilde{Y}_2^{\text{IR}}$. The graviton KK masses are determined by Eq. (13) with $\alpha = 2$.

2.2. 5D Propagators: the gauge field case

Let us consider the Green’s function of the quadratic operator for a gauge boson. We add to the action (2) a gauge fixing term [18]

$$\mathcal{L}_{g.f.} = -\frac{1}{2\xi} a(z) \left\{ \partial_\mu A^\mu - \xi a(z)^{-1} \partial_z [a(z) A^5] \right\}^2 , \quad (21)$$

where ξ is the gauge fixing parameter. Working in mixed position/momentum space [29], the propagator takes the form

$$-iP_p(z, z') \mathcal{P}_{\mu\nu} - iP_{\frac{p}{\sqrt{\epsilon}}}(z, z') \frac{p_\mu p_\nu}{p^2} , \quad (22)$$

where $\mathcal{P}^{\mu\nu} = \eta^{\mu\nu} - p^\mu p^\nu / p^2$ is the transverse projector, and $P_p(z, z')$ satisfies

$$O(p, z) P_p(z, z') = \delta(z - z') , \quad (23)$$

with $O(p, z)$ given by Eq. (4). $P_p(z, z')$ satisfies the same boundary conditions as the gauge field wavefunctions $f_n(z)$, Eqs. (9) and (10); for the inclusion of brane localized terms, see [21]. On the IR brane, we take $m_{\text{IR}} \equiv m$ in Eq. (11). For the UV b.c. we will choose simple Neumann or Dirichlet (i.e. $b_{\text{UV}} = 0$ or $b_{\text{UV}} \rightarrow \infty$):

$$\partial_z P_p^N(z, z') \Big|_{z=L_0} = 0 \quad P_p^D(z, z') \Big|_{z=L_0} = 0 . \quad (24)$$

The two solutions can be written in terms of two functions, denoted $K_m(p, z)$ and $S(p, z)$ [30], that satisfy the homogeneous differential equation

$$O(p, z) K_m(p, z) = O(p, z) S(p, z) = 0 , \quad (25)$$

and boundary conditions

$$K_m(p, L_0) = 1 , \quad L_0 K'_m(p, L_1) + a_1 b_{\text{IR}} K_m(p, L_1) = 0 , \quad (26)$$

$$S(p, L_0) = 0 , \quad S'(p, L_0) = 1 , \quad (27)$$

where a prime denotes derivative with respect to z . The Green’s functions read

$$P_p^N(z, z') = \frac{K_m(p, z_{<}) K_m(p, z_{>})}{K'_m(p, L_0)} - S(p, z_{<}) K_m(p, z_{>}) , \quad (28)$$

$$P_p^D(z, z') = -S(p, z_{<}) K_m(p, z_{>}) , \quad (29)$$

where $z_{<}$ and $z_{>}$ are the minimum and maximum of z and z' , respectively. The explicit solutions for K_m and S are given in Eqs. (A.1) and (A.4) of the appendix. The full propagators read

$$P_p(z, z') = \frac{\pi}{2} \frac{z_{<} z_{>}}{L_0} \frac{(\tilde{Y}_1^{\text{UV}} J_1^{z_{<}} - \tilde{J}_1^{\text{UV}} Y_1^{z_{<}})(\tilde{Y}_1^{\text{IR}} J_1^{z_{>}} - \tilde{J}_1^{\text{IR}} Y_1^{z_{>}})}{\tilde{J}_1^{\text{UV}} \tilde{Y}_1^{\text{IR}} - \tilde{Y}_1^{\text{UV}} \tilde{J}_1^{\text{IR}}} , \quad (30)$$

where we used the notation for the Bessel functions of Eqs. (5) and (12) with $m_n \rightarrow p$, and $b_{\text{UV}} = 0$ for $P_p^N(z, z')$ while $b_{\text{UV}} \rightarrow \infty$ for $P_p^D(z, z')$.

We have split the Neumann propagator in Eq. (28) in two pieces, one that vanishes at the UV brane and exactly coincides with the Dirichlet propagator, Eq. (29), and another that is the product of the holographic functions times the boundary field two point function, to be introduced in Section 3.2. Alternatively, we can separate it into the contribution from the massless zero mode (before EWSB) and that of the massive modes

$$P_p(z, z') = P_p^{(0)}(z, z') + \tilde{P}_p(z, z') , \quad (31)$$

where the Green's function for the zero mode reads

$$P_p^{(0)} = \frac{1}{p^2 L_0 \log \frac{L_1}{L_0}} , \quad (32)$$

and, for simplicity, we set $r_{\text{UV}} = r_{\text{IR}} = 0$ (see [20, 21, 31] for a thorough discussion of the phenomenological consequences of localized gauge kinetic terms). Propagator methods are also useful for resumming the effects of the fermion KK tower (see e.g. [32]).

2.3. Holographic method

Let us consider a bulk gauge boson A_M with the following action

$$S_{\text{gauge}} = \int \frac{d^4 p}{(2\pi)^4} dz \sqrt{g} \left\{ -\frac{1}{4g_{5A}^2} (A_{MN})^2 + \frac{1}{2} v^2(z) (A_M)^2 \right\} , \quad (33)$$

where we allow for a bulk Higgs vev profile, $v(z)$, with mass dimension 3/2. ¶ We will go to a gauge with $A_5 = 0$ and assume that the gauge boson obeys Neumann b.c.'s on the UV brane. We write the 5D field as follows

$$A_\mu(p, z) = f_A(p, z) \bar{A}_\mu(p) , \quad (34)$$

with $f_A(p, L_0) = 1$ so that $\bar{A}_\mu(p)$ is the boundary value of the gauge field. The IR boundary condition is the same as for the 5D field. We assume the boundary field satisfies the equation of motion of a four-dimensional gauge field, which implies the following equation for the holographic profile

$$O_A f_A(p, z) = 0 , \quad (35)$$

where $O_A = O(p, z) + a(z)^3 g_{5A}^2 v^2(z)$ with $O(p, z)$ as defined in Eq. (4). The effective action for the boundary field can be obtained at tree level and to quadratic order in the fields by inserting the equations of motion back in the action and integrating over the extra dimension. The bulk action vanishes due to the equations of motion and the only remaining term is a boundary piece that reads

$$S_{\text{bound.}} = -\frac{1}{2} \int \frac{d^4 p}{(2\pi)^4} \bar{A}_\mu \bar{\Pi}_A \bar{A}^\mu , \quad (36)$$

¶ For EWSB localized on the IR brane, $v^2(z) \equiv \frac{1}{2} [v/a(L_1)]^2 a(z)^{-1} \delta(z - L_1)$, which gives $m = \frac{1}{2} g_{5A}^2 [v/a(L_1)]^2$ in Eqs. (25)-(27). We introduce the factors of 1/2 and $1/a(L_1)$ to match to the $SU(2) \times U(1)_Y$ theory with $v \sim 174$ GeV.

with the vacuum polarization function for the boundary field given by

$$\bar{\Pi}_A(p^2) = \frac{1}{g_{5A}^2} \partial_z f_A(p^2, z) \Big|_{z=L_0} . \quad (37)$$

Fermions can be treated in a similar way. The action for a bulk fermion is as in Eq. (14) but with an additional UV localized term [33]

$$\delta S_{\text{UV}} = \int_{\text{UV}} d^4x \sqrt{g_{\text{ind}}} \left(\pm \frac{1}{2} \right) \bar{\Psi} \Psi , \quad (38)$$

where g_{ind} is the induced metric, and the factor of $+1/2$ ($-1/2$) is determined by the requirement that the LH (RH) chirality be unconstrained on the UV brane. We assume the LH component satisfies Neumann b.c.'s on the UV brane and adopt a LH source description

$$\Psi_{L,R}(p, z) = f_{L,R}(p, z) \psi_{L,R}(p) , \quad (39)$$

where $\not{p} \psi_{L,R}(p) = p \psi_{R,L}(p)$ and $f_{L,R}$ satisfy the equations

$$O_{-c} O_c f_L = -p^2 f_L , \quad O_c f_L = p f_R , \quad (40)$$

where O_c is given in Eq. (16). The boundary conditions on the IR brane are as for the 5D field, while on the UV brane we impose

$$f_L(p, L_0) = 1 . \quad (41)$$

The boundary action for ψ_L is computed by replacing the classical equations of motion and integrating over the extra dimension. Again, at the quadratic level there is no bulk contribution and the boundary contribution, Eq. (38), simply reads

$$S_{\text{bound.}} = \int \frac{d^4p}{(2\pi)^4} \bar{\psi}_L \not{p} \Sigma(p) \psi_L , \quad (42)$$

where the kinetic function for the boundary field is

$$\Sigma(p) = \frac{f_R(p, L_0)}{p} , \quad (43)$$

where we have used $\Psi_R(p, L_0) = f_R(p, L_0) (\not{p}/p) \psi_L$. Canonical normalization is obtained by the field redefinition $\tilde{\psi}_L = \sqrt{\Sigma(p)} \psi_L$. In the limit of zero momentum we get $\tilde{\psi}_L \xrightarrow{p \rightarrow 0} \psi_L / f_L^0(L_0)$, where $f_L^0(z)$ is the fermion zero-mode wavefunction, Eq. (18), and $\tilde{\psi}_L$ has 4D mass dimension, $[\tilde{\psi}_L] = 3/2$.

The explicit solutions for the gauge and fermion holographic profiles, $f_A(p, z)$ and $f_L(p, z)$, are given in Eqs. (A.1) and (A.6) of the appendix, respectively.

2.4. Relation between the methods

The three methods we have reviewed in the previous sections are related to each other. The 5D propagator can be written in terms of the KK expansion as

$$P_p(z, z') = \sum_n \frac{f_n(z) f_n(z')}{p^2 - m_n^2} . \quad (44)$$

Similarly, the boundary kinetic function in the holographic method is given by the inverse of the (Neumann) boundary to boundary propagator

$$\partial_z f_A(p, L_0) = \frac{1}{P_p^N(L_0, L_0)} = K'_m(p, L_0) , \quad (45)$$

where in the second equality we used Eq. (28) for the case that the EWSB mass m is IR brane localized, together with the b.c.'s (26) and (27). The holographic profile itself, $f_A(p, z)$, is given by the amputated bulk to boundary propagator, where amputation means dividing by the boundary to boundary propagator

$$f_A(p, z) = \frac{P_p^N(L_0, z)}{P_p^N(L_0, L_0)} = K_m(p, z) . \quad (46)$$

In particular, both the holographic functions and the 5D propagator contain information on the whole spectrum, which can be extracted by evaluating the residue of the corresponding functions on-shell (they have poles at the corresponding masses of the physical particles). Eq. (44) shows that the 5D propagators resum the contribution of the whole tower of KK modes and are therefore rather efficient when computing indirect effects of the massive modes. The holographic method also resums the effect of the whole tower, although it does so in a different basis which can be very useful in certain situations as we will review below.

3. Low-energy effective Lagrangian

3.1. Integrating out gauge boson KK modes with 5D propagators

We start our discussion of electroweak tests of models with warped extra dimensions by introducing the prototype of realistic model [15, 16] and computing its low energy effective Lagrangian. In the following sections we show how to use different techniques to obtain the same effective Lagrangian and study the constraints on the model from electroweak precision data. The model has a bulk $SU(2)_L \times SU(2)_R \times U(1)_X$ gauge symmetry, broken by boundary conditions to the SM gauge symmetry $SU(2)_L \times U(1)_Y$ on the UV brane. Separating the gauge fields into zero modes and massive modes, the full covariant derivative can be written as

$$D_\mu^{\text{full}} = D_\mu - i \left[g_{5L} \tilde{L}_\mu^a T_L^a + g_{5R} \tilde{R}_\mu^b T_R^b + g'_{5Y} \tilde{B}_\mu + g_{5Z'} Q_{Z'} \tilde{Z}'_\mu \right] , \quad (47)$$

where D_μ represents the SM covariant derivative (in 4D momentum space) and we use tildes to denote the massive KK components of the 5D fields. Here $a = 1, 2, 3$, $b = 1, 2$, L_μ^a and R_μ^a are the gauge fields corresponding to $SU(2)_L$ and $SU(2)_R$, respectively, and we have defined the hypercharge and Z' gauge bosons as

$$B_\mu = \frac{g_{5X} R_\mu^3 + g_{5R} X_\mu}{\sqrt{g_{5R}^2 + g_{5X}^2}} , \quad Z'_\mu = \frac{g_{5R} R_\mu^3 - g_{5X} X_\mu}{\sqrt{g_{5R}^2 + g_{5X}^2}} . \quad (48)$$

We have denoted with g_{5L} , g_{5R} and g_{5X} the five-dimensional gauge couplings of the three bulk gauge groups. The corresponding couplings of the hypercharge and Z' read

$$g'_5 = \frac{g_{5R} g_{5X}}{\sqrt{g_{5R}^2 + g_{5X}^2}} , \quad g_{5Z'} = \sqrt{g_{5R}^2 + g_{5X}^2} , \quad (49)$$

with charges

$$Y = T_R^3 + Q_X , \quad Q_{Z'} = \frac{g_{5R}^2 T_R^3 - g_{5X}^2 Q_X}{g_{5R}^2 + g_{5X}^2} , \quad (50)$$

so that the electric charge is $Q = T_L^3 + T_R^3 + Q_X$.

Our goal in this section is to compute the low energy effective Lagrangian for this model. We will do so at tree level, assuming there is a light Higgs in the spectrum. The effective Lagrangian can be obtained at tree level by solving the equations of motion of the heavy particles and replacing the solutions back in the Lagrangian. The 5D Lagrangian, omitting tensor indices, can be written as

$$\begin{aligned} \mathcal{L}_5 = \mathcal{L}_{SM} - \frac{1}{2} \tilde{L}^a O \tilde{L}^a - \frac{1}{2} \tilde{R}^b O \tilde{R}^b - \frac{1}{2} \tilde{B} O \tilde{B} - \frac{1}{2} \tilde{Z}' O \tilde{Z}' \\ + g_{5L} \tilde{J}^{aL} \tilde{L}^a + g'_5 \tilde{J}^Y \tilde{B} + g_{5R} \tilde{J}^{bR} \tilde{R}^b + g_{5Z'} \tilde{J}^{Z'} \tilde{Z}' + \dots , \end{aligned} \quad (51)$$

where $O = O(p, z)$ was defined in Eq. (4), and the dots denote interaction terms with more than one heavy field which, in the case of gauge bosons, do not give contributions to the effective Lagrangian at leading order. We have defined the effective currents

$$\tilde{J}_\mu^{aL} = [a^3 (f_h^0)^2 J_{h\mu}^{aL} + a^4 \sum_\psi (f_L^0)^2 J_{\psi\mu}^{aL}] , \quad \tilde{J}_\mu^{bR} = [a^3 (f_h^0)^2 J_{h\mu}^{bR} + a^4 \sum_\psi (f_L^0)^2 J_{\psi\mu}^{bR}] , \quad (52)$$

$$\tilde{J}_\mu^Y = [a^3 (f_h^0)^2 J_{h\mu}^Y + a^4 \sum_\psi (f_L^0)^2 J_{\psi\mu}^Y] , \quad \tilde{J}_\mu^{Z'} = [a^3 (f_h^0)^2 J_{h\mu}^{Z'} + a^4 \sum_\psi (f_L^0)^2 J_{\psi\mu}^{Z'}] , \quad (53)$$

where f_L^0 is the wave function of the fermion zero modes as defined in Eq. (18), the Higgs wavefunction f_h^0 is normalized as in Eq. (7) with $f_n(z) \rightarrow L^{1/2} a(z) f_h^0(z)$ ⁺, and the fermionic currents are

$$J_\psi^{aL,R\mu} \equiv \bar{\psi} \gamma^\mu T_{L,R}^a \psi , \quad J_\psi^{Y\mu} \equiv \bar{\psi} \gamma^\mu Y \psi , \quad J_\psi^{Z'\mu} \equiv \bar{\psi} \gamma^\mu Q_{Z'} \psi , \quad (54)$$

while the Higgs currents are

$$J_{h\mu}^{aL,R} \equiv h^\dagger T_{L,R}^a i D_\mu h + \text{h.c.} , \quad J_{h\mu}^Y \equiv h^\dagger Y i D_\mu h + \text{h.c.} , \quad J_{h\mu}^{Z'} \equiv h^\dagger Q_{Z'} i D_\mu h + \text{h.c.} \quad (55)$$

We can now integrate out the heavy fields by replacing back in the Lagrangian the solution of the classical equations of motion, which can be written in terms of the Green's function of the corresponding differential operator [see Eqs. (28)-(32)] as

$$\tilde{L}^a(z) = g_{5L} \int_{L_0}^{L_1} dz' \tilde{P}_p^N(z, z') \tilde{J}^{aL} , \quad \tilde{B}(z) = g'_5 \int_{L_0}^{L_1} dz' \tilde{P}_p^N(z, z') \tilde{J}^Y , \quad (56)$$

for the fields that are unbroken on the UV brane, and

$$\tilde{R}^b(z) = g_{5R} \int_{L_0}^{L_1} dz' \tilde{P}_p^D(z, z') \tilde{J}^{bR} , \quad \tilde{Z}'(z) = g_{5Z'} \int_{L_0}^{L_1} dz' \tilde{P}_p^D(z, z') \tilde{J}^{Z'} , \quad (57)$$

for those that vanish on the UV brane. The Neumann (with the zero mode subtracted) or Dirichlet propagator takes care of the corresponding boundary conditions on the UV brane. Also, the propagators are computed in the EW preserving vacuum [e.g., for an

⁺ For instance, in models of Gauge-Higgs unification one has $f_h^0(z) = \sqrt{2/[L_0(L_1^2/L_0^2 - 1)]} a(z)^{-2}$. For an IR brane localized Higgs: $a^3(z)[f_h(z)]^2 = \delta(z - L_1)$.

IR localized Higgs, $m = 0$ in Eq. (30)]. The resulting effective Lagrangian can be put in the standard basis of [34] by using the equations of motion of the SM fields. It reads

$$\mathcal{L}_{\text{eff}} = \mathcal{L}_{\text{SM}} + \alpha_h \mathcal{O}_h + \sum_{\psi_L} \alpha_{h\psi_L}^t \mathcal{O}_{h\psi_L}^t + \sum_{\psi} \alpha_{h\psi}^s \mathcal{O}_{h\psi}^s + \sum_{\psi_L, \psi'_L} \alpha_{\psi_L \psi'_L}^t \mathcal{O}_{\psi_L \psi'_L}^t + \sum_{\psi, \psi'} \alpha_{\psi \psi'}^s \mathcal{O}_{\psi \psi'}^s, \quad (58)$$

where ψ_L stands for any of the SM LH doublets, ψ for any of the SM fermion fields, the gauge fields in \mathcal{L}_{SM} are assumed to be canonically normalized, and the different operators are defined as follows (\mathcal{O}_{WB} is not induced at tree level in this basis):

- Oblique operators

$$\mathcal{O}_h = |h^\dagger D_\mu h|^2, \quad \mathcal{O}_{WB} = (h^\dagger \sigma^a h) W_{\mu\nu}^a B^{\mu\nu}. \quad (59)$$

- Two-fermion operators

$$\mathcal{O}_{h\psi}^s = i(h^\dagger D_\mu h)(\bar{\psi} \gamma^\mu \psi) + \text{h.c.}, \quad \mathcal{O}_{h\psi_L}^t = i(h^\dagger \sigma^a D_\mu h)(\bar{\psi}_L \gamma^\mu \sigma^a \psi_L) + \text{h.c.} \quad (60)$$

- Four-fermion operators

$$\mathcal{O}_{\psi\psi'}^s = \frac{1}{1 + \delta_{\psi\psi'}} (\bar{\psi} \gamma^\mu \psi)(\bar{\psi}' \gamma_\mu \psi'), \quad \mathcal{O}_{\psi_L \psi'_L}^t = \frac{1}{1 + \delta_{\psi_L \psi'_L}} (\bar{\psi}_L \gamma^\mu \sigma^a \psi_L)(\bar{\psi}'_L \gamma_\mu \sigma^a \psi'_L). \quad (61)$$

The coefficients α_i , which encode the dependence on the model parameters, read

$$\alpha_h = \frac{\bar{g}'^2}{2} [\alpha^N - \alpha^D], \quad (62)$$

$$\alpha_{h\psi_L}^t = \frac{\bar{g}_L^2}{4} \beta_{\psi_L}^N, \quad (63)$$

$$\alpha_{h\psi}^s = \frac{\bar{g}'^2}{2} Y_\psi \beta_\psi^N + \frac{\bar{g}_R^2 T_R^3(\psi) - \bar{g}'^2 Y_\psi}{2} \beta_\psi^D, \quad (64)$$

$$\alpha_{\psi_L \psi'_L}^t = \frac{\bar{g}_L^2}{4} \gamma_{\psi_L \psi'_L}^N, \quad (65)$$

$$\alpha_{\psi\psi'}^s = \bar{g}'^2 Y_\psi Y_{\psi'} \gamma_{\psi\psi'}^N + \frac{[\bar{g}_R^2 T_R^3(\psi) - \bar{g}'^2 Y_\psi][\bar{g}_R^2 T_R^3(\psi') - \bar{g}'^2 Y_{\psi'}]}{\bar{g}_R^2 - \bar{g}'^2} \gamma_{\psi\psi'}^D, \quad (66)$$

where $\bar{g}_{L,R}^2 = g_{5,L,R}^2/L$ and $\bar{g}'^2 = g_5'^2/L$, with L the volume factor (8), while Y_ψ and $T_R^3(\psi)$ are the hypercharge and third component of $SU(2)_R$ isospin for the field ψ , respectively (for the SM fermions, $Y_q = 1/6$, $Y_u = 2/3$, $Y_d = -1/3$, $Y_l = -1/2$, $Y_e = -1$). The parameters $\alpha^{N,D}, \beta_\psi^{N,D}, \gamma_{\psi\psi'}^{N,D}$ are defined as

$$\alpha^{N,D} = L \int_{L_0}^{L_1} dz dz' a^3(z) [f_h^0(z)]^2 \tilde{P}_p^{N,D}(z, z') a^3(z) [f_h^0(z)]^2, \quad (67)$$

$$\beta_\psi^{N,D} = L \int_{L_0}^{L_1} dz dz' a^4(z) [f_\psi^0(z)]^2 \tilde{P}_p^{N,D}(z, z') a^3(z) [f_h^0(z)]^2, \quad (68)$$

$$\gamma_{\psi\psi'}^{N,D} = L \int_{L_0}^{L_1} dz dz' a^4(z) [f_\psi^0(z)]^2 \tilde{P}_p^{N,D}(z, z') a^4(z) [f_{\psi'}^0(z)]^2. \quad (69)$$

Since we are interested in the contribution of dimension-6 operators, we can evaluate the 5D propagators at zero momentum,

$$\tilde{P}_0^N(z, z') = \frac{z_{<}^2 \left(1 + 2 \log \frac{L_0}{z_{<}}\right) + z_{>}^2 \left(1 + 2 \log \frac{L_1}{z_{>}}\right) - \frac{L_1^2}{\log \frac{L_1}{L_0}}}{4L_0 \log \frac{L_1}{L_0}}, \quad (70)$$

$$\tilde{P}_0^D(z, z') = \frac{L_0}{2} \left(1 - \frac{z_{<}^2}{L_0^2}\right). \quad (71)$$

Note that, although we have put a tilde on the Dirichlet propagator, there is no zero mode subtraction in that case.

The above results provide the dimension-6 effective Lagrangian for general models in warped extra dimensions with custodial symmetry and a light Higgs, after integration of the gauge boson heavy modes. * Simple limits can be easily obtained from this general Lagrangian. For instance, if we consider that the bulk symmetry is just the SM one, we obtain, by setting to zero the Dirichlet coefficients, the following effective Lagrangian

$$\begin{aligned} \mathcal{L}_{\text{eff}} = \mathcal{L}_{SM} + \frac{\bar{g}^2}{2} \left[\alpha^N J_h^{aL\mu} J_{h\mu}^{aL} + 2 \sum_{\psi} \beta_{\psi}^N J_h^{aL\mu} J_{\psi\mu}^{aL} + \sum_{\psi, \psi'} \gamma_{\psi\psi'}^N J_{\psi}^{aL\mu} J_{\psi'\mu}^{aL} \right] \\ + \frac{\bar{g}'^2}{2} \left[\alpha^N J_h^{Y\mu} J_{h\mu}^Y + 2 \sum_{\psi} \beta_{\psi}^N J_h^{Y\mu} J_{\psi\mu}^Y + \sum_{\psi, \psi'} \gamma_{\psi\psi'}^N J_{\psi}^{Y\mu} J_{\psi'\mu}^Y \right] + \dots \quad (72) \end{aligned}$$

Note that the Dirichlet terms involving fermions vanish in the limit of UV localized fermions. Thus, the above Lagrangian, with the replacement $\alpha^N \rightarrow \alpha^N - \alpha^D$, is also the effective Lagrangian of models with custodial symmetry and UV localized fermions.

In the case that the Higgs field is localized on the IR brane, $a^3(z)[f_h(z)]^2 = \delta(z - L_1)$, these coefficients are explicitly given by

$$\alpha^N = \frac{L_1^2}{4} \left[-2 \log \frac{L_1}{L_0} + 2 - \frac{1}{\log \frac{L_1}{L_0}} \right] , \quad (73)$$

$$\beta_{\psi}^N = \frac{L_1^2}{4} \left[1 - \frac{1}{\log \frac{L_1}{L_0}} + g_2(c_{\psi}) \left(1 - 2 \log \frac{L_1}{L_0} \right) - 2\tilde{g}_2(c_{\psi}) \right] , \quad (74)$$

where c_{ψ} is the bulk mass parameter for the fermion ψ and the auxiliary functions $g_n(c)$ and $\tilde{g}_n(c)$ are defined in Eqs. (A.7) and (A.8) of the appendix. Finally γ^N is a complicated function of c_{ψ} and $c_{\psi'}$. In the limit $c \rightarrow \infty$ (UV localized fermions) it simplifies to

$$\gamma^N(c \rightarrow \infty) = -\frac{L_1^2}{4 \log \frac{L_1}{L_0}} . \quad (75)$$

Also, for future reference, when the Higgs is localized on the IR brane

$$\alpha^D = -\frac{L_1^2}{2} \log \frac{L_1}{L_0} , \quad \beta_{\psi}^D = -\frac{L_1^2}{2} \log \frac{L_1}{L_0} g_2(c_{\psi}) . \quad (76)$$

3.1.1. Universal case An assumption that significantly simplifies the analysis of EWPT is that of universal new physics [37]. Models of universal new physics are those for which a combination of gauge bosons exists (so called interpolating fields) \bar{W}^a , with $a = 1, 2, 3$, and \bar{B} such that the only couplings of fermions (excluding Yukawa couplings) are of the form

$$\mathcal{L}_{\text{fermions}}^{\text{Univ.}} = \bar{W}_{\mu}^a J_f^{aL\mu} + \bar{B}_{\mu} J_f^{Y\mu} + \dots , \quad (77)$$

* The integration of fermion heavy modes can be performed trivially from the general results in [35], see for instance [36].

where the dots denote kinetic and Yukawa terms for the fermions. In particular, the interpolating fields \bar{W}^a and \bar{B} are not canonically normalized. The SM fermionic currents are defined by [see Eq. (54)]

$$J_f^{aL\mu} \equiv \sum_{\psi} J_{\psi}^{aL\mu}, \quad J_f^{Y\mu} \equiv \sum_{\psi} J_{\psi}^{Y\mu}. \quad (78)$$

In this case, all relevant contributions to EWPT can be encoded in the vacuum polarizations of the interpolating fields (oblique corrections). Assuming unbroken QED, the quadratic Lagrangian for the interpolating fields, together with the gauge-fermion interactions, can be written as

$$\begin{aligned} \mathcal{L}_{\text{Oblique}} = & -\mathcal{P}^{\mu\nu} \left[\bar{W}_{\mu}^+ \bar{\Pi}_{+-}(p^2) \bar{W}_{\nu}^- + \frac{1}{2} \bar{W}_{\mu}^3 \bar{\Pi}_{33}(p^2) \bar{W}_{\nu}^3 \right. \\ & \left. + \frac{1}{2} \bar{B}_{\mu} \bar{\Pi}_{BB}(p^2) \bar{B}_{\nu} + \bar{W}_{\mu}^3 \bar{\Pi}_{3B}(p^2) B_{\nu} \right] + \mathcal{L}_{\text{fermions}}^{\text{Univ.}}, \end{aligned} \quad (79)$$

where $\mathcal{P}^{\mu\nu}$ is the transverse projector and we have defined $\bar{W}^{\pm} \equiv (\bar{W}^1 \mp i\bar{W}^2)/\sqrt{2}$.

In the case that the coefficients $\beta_{\psi}^N \equiv \beta$ and $\gamma_{\psi\psi'}^N \equiv \gamma$ in Eq. (72) are independent of the fermion type, ψ , the effective Lagrangian takes the form

$$\begin{aligned} \mathcal{L}_{\text{eff}} = \mathcal{L}_{SM} + \frac{\bar{g}^2}{2} & \left[\alpha J_h^{aL\mu} J_{h\mu}^{aL} + 2\beta J_h^{aL\mu} J_{f\mu}^{aL} + \gamma J_f^{aL\mu} J_{f\mu}^{aL} \right] \\ & + \frac{\bar{g}'^2}{2} \left[\alpha J_h^{Y\mu} J_{h\mu}^Y + 2\beta J_h^{Y\mu} J_{f\mu}^Y + \gamma J_f^{Y\mu} J_{f\mu}^Y \right] + \dots \end{aligned} \quad (80)$$

This effective Lagrangian is not in oblique form, since it includes corrections to the fermion gauge couplings and four-fermion interactions, proportional to β and γ , respectively. The corrections are however universal and can be written purely in terms of oblique corrections. This can be done in two equivalent ways, either by using the classical equations of motion of the SM fields as determined by \mathcal{L}_{SM} or by doing field redefinitions that eliminate the corrections involving fermions. The latter approach consists of performing a shift of the gauge fields, proportional to the fermion currents that eliminates the four-fermion terms, followed by a gauge field rescaling that puts the fermion-gauge interactions in the form of Eq. (77). Replacing a Higgs vev $\langle h \rangle = (0, v)$ in the Higgs currents (55), the field redefinitions are, to first order in α , β and γ :

$$W^a = \frac{1}{\bar{g}} \bar{W}^a \left[1 - \frac{\bar{g}^2 v^2}{2} \beta - \frac{\gamma}{2} \Pi_{aa}^{\text{SM}} \right] - \frac{\bar{g}}{2} \gamma J_f^{aL} + \delta^{a3} \frac{1}{\bar{g}'} \bar{B} \left[\frac{\bar{g}\bar{g}' v^2}{2} \beta - \frac{\gamma}{2} \Pi_{3B}^{\text{SM}} \right], \quad (81)$$

$$B = \frac{1}{\bar{g}'} \bar{B} \left[1 - \frac{\bar{g}'^2 v^2}{2} \beta - \frac{\gamma}{2} \Pi_{BB}^{\text{SM}} \right] - \frac{\bar{g}'}{2} \gamma J_f^Y + \frac{1}{\bar{g}} \bar{W}^3 \left[\frac{\bar{g}\bar{g}' v^2}{2} \beta - \frac{\gamma}{2} \Pi_{3B}^{\text{SM}} \right], \quad (82)$$

where the vacuum polarization functions in the SM limit are defined by

$$\Pi_{aa}^{\text{SM}} = p^2 - \frac{\bar{g}^2 v^2}{2}, \quad \Pi_{BB}^{\text{SM}} = p^2 - \frac{\bar{g}'^2 v^2}{2}, \quad \Pi_{3B}^{\text{SM}} = \frac{\bar{g}\bar{g}' v^2}{2}. \quad (83)$$

These field redefinitions lead to an oblique form for the effective Lagrangian written in terms of the interpolating fields \bar{W}^a, \bar{B} , as in Eq. (79), with the following vacuum polarization functions

$$\bar{g}^2 \bar{\Pi}_{aa} = \Pi_{aa}^{\text{SM}} (1 - \bar{g}^2 v^2 \beta - \gamma \Pi_{aa}^{\text{SM}}) - \frac{\bar{g}^2 v^4}{4} (\bar{g}^2 + \delta_{a3} \bar{g}'^2) \alpha + \delta_{a3} \Pi_{3B}^{\text{SM}} (\bar{g}\bar{g}' v^2 \beta - \gamma \Pi_{3B}^{\text{SM}})$$

$$= -\frac{\bar{g}^2 v^2}{2} \left[1 - \left(\frac{\bar{g}^2}{\bar{g}'^2} + \delta_{a3} \right) \hat{T}^{\text{Op}} \right] + (1 - \hat{S}^{\text{Op}}) p^2 + \frac{2}{\bar{g}^2 v^2} W^{\text{Op}} p^4 + \dots, \quad (84)$$

$$\begin{aligned} \bar{g}'^2 \bar{\Pi}_{BB} &= \Pi_{BB}^{SM} (1 - \bar{g}'^2 v^2 \beta - \gamma \Pi_{BB}^{SM}) - \frac{\bar{g}'^2 v^4}{4} (\bar{g}^2 + \bar{g}'^2) \alpha + \Pi_{3B}^{SM} (\bar{g} \bar{g}' v^2 \beta - \gamma \Pi_{3B}^{SM}) \\ &= -\frac{\bar{g}'^2 v^2}{2} \left[1 - \left(\frac{\bar{g}^2}{\bar{g}'^2} + 1 \right) \hat{T}^{\text{Op}} \right] + \left(1 - \frac{\bar{g}'^2}{\bar{g}^2} \hat{S}^{\text{Op}} \right) p^2 + \frac{2}{\bar{g}^2 v^2} W^{\text{Op}} p^4 + \dots, \end{aligned} \quad (85)$$

$$\begin{aligned} \bar{g} \bar{g}' \bar{\Pi}_{3B} &= \Pi_{3B}^{SM} \left[1 - \frac{v^2}{2} (\bar{g}^2 + \bar{g}'^2) \beta - \gamma \Pi_{33BB} \right] + \frac{\bar{g} \bar{g}' v^2}{2} \left[\frac{v^2}{2} (\bar{g}^2 + \bar{g}'^2) \alpha + \beta \Pi_{33BB} \right] \\ &= \frac{\bar{g} \bar{g}' v^2}{2} \left[1 - \left(\frac{\bar{g}^2}{\bar{g}'^2} + 1 \right) \hat{T}^{\text{Op}} \right] + \frac{\bar{g}'}{\bar{g}} \hat{S}^{\text{Op}} p^2 + \dots, \end{aligned} \quad (86)$$

where $\Pi_{33BB} \equiv \Pi_{33}^{SM} + \Pi_{BB}^{SM}$, and in the second equality of each definition we expanded for small p^2 and wrote the result in terms of

$$\hat{T}^{\text{Op}} \equiv \frac{\bar{g}'^2 v^2}{2} (-\alpha + 2\beta - \gamma), \quad \hat{S}^{\text{Op}} \equiv \bar{g}^2 v^2 (\beta - \gamma), \quad W^{\text{Op}} \equiv -\frac{\bar{g}^2 v^2}{2} \gamma, \quad (87)$$

which will be identified in Section 4 as the oblique parameters of [37]. Recall that these same vacuum polarization functions represent also the effective Lagrangian of a custodially symmetric model with fermions localized on the UV brane if we make the replacement $\alpha \rightarrow \alpha^N - \alpha^D$.

3.2. Holographic method

In this section we rederive the effective Lagrangian of the model with custodial symmetry using the holographic method (for further discussions of holography, see the review in [38]). We consider first the case of UV localized fermions, which is the situation in which the holographic method is the most efficient, as it produces with minimal effort the effective Lagrangian in oblique form. In Subsection 3.2.1 we discuss how the formalism changes when fermions are allowed to propagate in the bulk.

In the presence of a bulk EWSB vev, $v(z)$, the gauge part of the action reads

$$\begin{aligned} S_{\text{gauge}}^{\text{Cust.}} &= \int \frac{d^4 p}{(2\pi)^4} dz \sqrt{g} \left\{ -\frac{1}{4g_{5L}^2} (L_{MN}^a)^2 - \frac{1}{4g_{5R}^2} (R_{MN}^a)^2 - \frac{1}{4g_{5X}^2} (X_{MN})^2 \right. \\ &\quad \left. + \frac{1}{2} v(z)^2 (L_M^a - R_M^a)^2 \right\} \\ &= \int \frac{d^4 p}{(2\pi)^4} dz \sqrt{g} \left\{ -\frac{1}{4g_{5Z}^2} (V_{MN}^a)^2 - \frac{1}{4g_{5Z}^2} (A_{MN}^a)^2 - \frac{1}{4g_{5X}^2} (X_{MN})^2 + \frac{1}{2} v(z)^2 A_M^2 \right\} \\ &\stackrel{\text{Hol}}{=} -\frac{1}{2} \int \frac{d^4 p}{(2\pi)^4} dz \sqrt{g} \left\{ \bar{A}^a \Pi_A(p^2) \bar{A}^a + \bar{V}^a \Pi_V(p^2) \bar{V}^a + \bar{X} \Pi_X(p^2) \bar{X} \right\}, \end{aligned} \quad (88)$$

where $g_{5Z}^2 \equiv g_{5L}^2 + g_{5R}^2$, and in the second equality we defined the axial and vector combinations

$$A_M^a = L_M^a - R_M^a, \quad V_M^a = \frac{g_{5R}}{g_{5L}} L_M^a + \frac{g_{5L}}{g_{5R}} R_M^a. \quad (89)$$

In the last line we used the holographic method (indicated by the $\stackrel{\text{Hol}}{=}$ symbol) to obtain the effective action for the fields evaluated on the UV brane:

$$\bar{A}^a = A^a(z = L_0) , \quad \bar{V}^a = V^a(z = L_0) , \quad \bar{X} = X(z = L_0) . \quad (90)$$

The corresponding vacuum polarizations read

$$\Pi_{A,V} = \frac{1}{g_{5Z}^2} \partial_z f_{A,V}(p^2, z = L_0) , \quad \Pi_X = \frac{1}{g_{5X}^2} \partial_z f_X(p^2, z = L_0) , \quad (91)$$

where f_A , f_V and f_X satisfy Eq. (35) with mass terms $M_A^2 = g_{5Z}^2 v^2$, $M_V^2 = 0$ and $M_X^2 = 0$, respectively. By assumption, the fermionic action is already localized on the UV brane. In particular, the coupling between the fermions and gauge bosons is universal, as in Eq. (77), with interpolating fields that are the 5D SM gauge boson fields evaluated at the UV brane. Replacing the boundary values of the axial, vector and X fields in terms of the SM ones \sharp

$$\bar{A}^a = \bar{W}_L^a - \delta^{a3} \bar{B} , \quad \bar{V}^a = \frac{g_R}{g_L} \bar{W}_L^a + \delta^{a3} \frac{g_L}{g_R} \bar{B} , \quad \bar{X} = \bar{B} , \quad (92)$$

we obtain an effective Lagrangian in the oblique form (79), with vacuum polarizations

$$\bar{\Pi}_{aa} = \Pi_A + \frac{g_{5R}^2}{g_{5L}^2} \Pi_V , \quad (93)$$

$$\bar{\Pi}_{BB} = \Pi_A + \frac{g_{5L}^2}{g_{5R}^2} \Pi_V + \Pi_X , \quad (94)$$

$$\bar{\Pi}_{3B} = -\Pi_A + \Pi_V . \quad (95)$$

Assuming that $v(z)^2 = (v^2/2)[f_h^0(z)]^2$, where the Higgs profile $f_h^0(z)$ is normalized as specified after Eq. (53), one can check that these vacuum polarization functions agree with the ones obtained using 5D propagators, Eqs. (84)-(86), up to a redefinition of the vev, $v^2 \rightarrow v^2[1 - \frac{1}{4}(g_{5L}^2 + g_{5R}^2)(v/a(L_1))^2 L_0]$, when expanded to the same order in v^2 and with the replacement $\alpha \rightarrow \alpha^N - \alpha^D$ to take into account the modifications due to the custodial symmetry. Note also that in the holographic formalism the custodial symmetry is explicit from Eq. (93), i.e. a symmetry between the charged and neutral W 's.

3.2.1. Holography with bulk fermions As we showed in the previous section, the holographic method is particularly suitable to compute the effective Lagrangian in the case of UV boundary localized fermions. The holographic method can still be used when the fermions propagate in the bulk although obtaining the effective Lagrangian requires more work. In this section we discuss the new steps one has to perform in the simple case of the SM bulk gauge symmetry, which can be obtained from our custodial model by setting $R_M^b = 0$, $R_M^3 = X_M = B_M$, and identifying the $U(1)_Y$ gauge coupling, g'_5 , as

\sharp Note the difference with respect to Eqs. (47) and (48) due to the non-canonical normalization of the fields in this section.

in Eq. (49). The gauge part of the Lagrangian then reads

$$S_{\text{gauge}} = \int \frac{d^4 p}{(2\pi)^4} dz \sqrt{g} \left\{ -\frac{1}{4g_5^2} (W_{MN}^b)^2 - \frac{1}{4g_{5Z}^2} [(A_{MN})^2 + (V_{MN})^2] \right. \\ \left. + \frac{1}{2} v(z)^2 [(W_M^b)^2 + (A_M)^2] \right\} \\ \stackrel{\text{Hol}}{=} -\frac{1}{2} \int \frac{d^4 p}{(2\pi)^4} \left\{ \bar{W}_\mu^b \Pi_W \bar{W}_b^\mu + \bar{A}_\mu \Pi_A \bar{A}^\mu + \bar{V}_\mu \Pi_V \bar{V}^\mu \right\} , \quad (96)$$

where

$$\Pi_{W,A,V} = \Pi(g_5^2 v^2, g_{5Z}^2 v^2, 0) , \quad (97)$$

and we indicate inside the parenthesis the masses to be used in Eqs. (35) and (37). Now we have $g_{5Z}^2 \equiv g_5^2 + g_5'^2$ and the following relation between the axial and vector fields, and the SM neutral ones:

$$A_M = W_M^3 - B_M , \quad V_M = \frac{g_5'}{g_5} W_M^3 + \frac{g_5}{g_5'} B_M , \quad (98)$$

so that the vacuum polarization functions for the SM boundary fields read

$$\Pi_{+-} = \Pi_W , \quad \Pi_{3B} = -\Pi_A + \Pi_V , \quad (99)$$

$$\Pi_{33} = \Pi_A + \frac{g_5'^2}{g_5^2} \Pi_V , \quad \Pi_{BB} = \Pi_A + \frac{g_5^2}{g_5'^2} \Pi_V . \quad (100)$$

As in the previous section, these would be the vacuum polarization functions for the interpolating fields for UV localized fermion fields. When the fermion fields live in the bulk, however, these terms do not give the full contribution to the boundary effective Lagrangian. Indeed there are both vertex and four-fermion interaction corrections as shown in Fig. 1. The left panel in the figure represents the vertex corrections. The

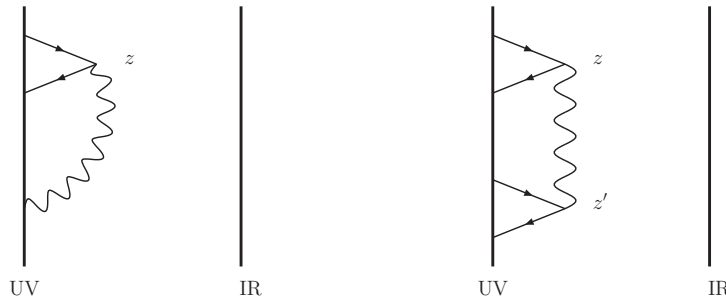


Figure 1. Vertex and four-fermion interaction contributions to the boundary action. The four-fermion interaction, with points at z and z' , is to be computed with the Dirichlet propagator, Eq. (29).

contribution to the effective Lagrangian is obtained by matching the corresponding amputated three point function in the full and effective theories. The diagram in the full theory requires bulk to boundary propagators for the gauge boson and fermions, and amputation means that the external legs are divided by the corresponding boundary to boundary propagators [= $g_5^2/K'_m(p^2, L_0)$ for the case of an IR brane localized

EWSB mass m , with g_5 and m the parameters of the corresponding gauge boson; see Eqs. (35), (37) and (45)]. Assuming fermion localization universality,^{††} the resulting extra contribution to the boundary action reads

$$S_{\text{Vertex}} = \int \frac{d^4 p}{(2\pi)^4} \left\{ \bar{g}_W \bar{W}_\mu^b \tilde{J}_f^{bL\mu} + \bar{g}_A \bar{A}_\mu \tilde{J}_Z^\mu + s_\theta c_\theta \bar{g}_V \bar{V}_\mu \tilde{J}_Q^\mu \right\}, \quad (101)$$

where $c_\theta = g_5/g_{5Z}$, $s_\theta = g'_5/g_{5Z}$, $\tilde{J}_Z^\mu = c_\theta^2 \tilde{J}_f^{3L\mu} - s_\theta^2 \tilde{J}_f^{Y\mu}$ and $\tilde{J}_Q^\mu = \tilde{J}_f^{3L\mu} + \tilde{J}_f^{Y\mu}$, with $\tilde{J}_f^{aL\mu}$ and $\tilde{J}_f^{Y\mu}$ as defined in Eqs. (78) and (54), but with $\psi \rightarrow \tilde{\psi}$ representing the canonically normalized boundary fermion fields (see end of Subsection 2.3). We also defined

$$\bar{f}_{W,V,A}(p^2) = \int_{L_0}^{L_1} dz a^4(z) [f_\psi^0(z)]^2 f_{W,V,A}(p^2, z), \quad (102)$$

where $f_{W,V,A}$ are the gauge boson “holographic” profiles associated with Eq. (97). Since we are interested in the couplings of the fermion zero modes, we have evaluated the corresponding fermion profiles at $p_\psi^2 = 0$ in (102) [neglecting the small fermion masses from EWSB], so that the zero-mode wavefunctions, Eq. (18), appear inside the integral, and there is dependence on a single momentum scale, associated with the gauge boson.

Bulk fermions also imply that four-fermion interactions are generated in the boundary action, due to the diagram in the right panel of Fig. 1. Again the coefficient in the effective theory is obtained by matching the amputated four-point function in the full and effective theories. On the full theory side, we use the Neumann bulk to bulk propagator and integrate over both interaction points. On the effective theory side, we have to use the boundary to boundary propagator using the couplings we have computed in Eq. (102). This latter term exactly coincides with the $K(z)K(z')/K'(L_0)$ part of full propagator, Eq. (28). The difference of the two therefore corresponds to computing the diagram on the right panel of Fig. 1 using the Dirichlet bulk to bulk propagator instead of the full one. The induced 4-fermion operators are

$$S_{4\text{-fermion}} = \int \frac{d^4 p}{(2\pi)^4} \left\{ \frac{g_5^2}{2L} \gamma_W^D \tilde{J}_{f\mu}^{bL} \tilde{J}_f^{bL\mu} + \frac{g_{5Z}^2}{2L} \gamma_A^D \tilde{J}_{Z\mu} \tilde{J}_Z^\mu + s_\theta^2 c_\theta^2 \frac{g_{5Z}^2}{2L} \gamma_V^D \tilde{J}_{Q\mu} \tilde{J}_Q^\mu \right\}, \quad (103)$$

where g_{5Z}^2 was defined after Eq. (97), L is the volume factor Eq. (8), and $\gamma_{W,A,V}^D$ were defined in Eq. (69), with the Dirichlet propagator corresponding to W , A and V (i.e. gauge boson squared masses $g_5^2 v^2$, $g_{5Z}^2 v^2$ and 0, respectively). If we are interested in the contribution to the effective Lagrangian up to operators of dimension 6, we can evaluate the corresponding propagator at zero momentum and neglect EWSB effects, i.e. use Eq. (71). In that case, $\gamma_W^D = \gamma_A^D = \gamma_V^D = \gamma^{\text{Hol}}$, and assuming universality we have

$$\gamma^{\text{Hol}} = \frac{L_1^2 \log \frac{L_1}{L_0} (3 - 2c) \left(\frac{L_0}{L_1}\right)^2 - (2c - 1)^2 \left(\frac{L_0}{L_1}\right)^{4c-2} + 8(c - 1) \left(\frac{L_0}{L_1}\right)^{2c+1}}{4 (2c^2 - 5c + 3) \left[1 - \left(\frac{L_0}{L_1}\right)^{2c-1}\right]^2}. \quad (104)$$

^{††}Eqs. (96), (101) and (103) below are trivially generalized to the non-universal case by expressing the results in terms of the individual fermion currents of Eqs. (78), and using the corresponding fermion profiles in Eqs. (102) and (69).

The effective Lagrangian given by Eqs. (96), (101) and (103) is not in the oblique form but can be rewritten in such a form due to the assumption of universality of fermion localization. The simplest way to proceed is to first shift the gauge fields as

$$\bar{W}^b \rightarrow \bar{W}^b - \frac{g_5^2}{2L\bar{g}_W} \gamma_W^D \tilde{J}_f^{bL}, \quad \bar{A} \rightarrow \bar{A} - \frac{g_{5Z}^2}{2L\bar{g}_A} \gamma_A^D \tilde{J}_Z, \quad \bar{V} \rightarrow \bar{V} - \frac{s_\theta c_\theta g_{5Z}^2}{2L\bar{g}_V} \gamma_V^D \tilde{J}_Q,$$

so as to eliminate the four-fermion interactions (to first order in the γ_i^D), followed by a rescaling $\bar{W}^b \rightarrow \bar{W}^b/\bar{g}_W$, $\bar{A} \rightarrow \bar{A}/\bar{g}_A$ and $\bar{V} \rightarrow \bar{V}/\bar{g}_V$, with

$$\bar{g}_i(p^2) = \bar{g}_i(p^2) \left[1 + \frac{g_{5i}^2}{2L\bar{g}_i^2(p^2)} \gamma_i \Pi_i(p^2) \right], \quad i = W, A, V, \quad (105)$$

where $g_{5i}^2 = g_5^2$ for $i = W$, $g_{5i}^2 = g_{5Z}^2$ for $i = A, V$, \bar{g}_i are given in Eq. (102), and Π_i are given in Eq. (97), for $i = W, A, V$. Expressing the resulting Lagrangian in terms of W^a and B , as in Eq. (98) one finds that the fermion couplings to the new gauge bosons are universal as in (77), while the vacuum polarizations are

$$\bar{\Pi}_{+-} = \frac{1}{\bar{g}_W^2} \Pi_W, \quad \bar{\Pi}_{33} = \frac{1}{\bar{g}_A^2} \Pi_A + \frac{1}{\bar{g}_V^2} \frac{g_5'^2}{g_5^2} \Pi_V, \quad (106)$$

$$\bar{\Pi}_{3B} = -\frac{1}{\bar{g}_A^2} \Pi_A + \frac{1}{\bar{g}_V^2} \Pi_V, \quad \bar{\Pi}_{BB} = \frac{1}{\bar{g}_A^2} \Pi_A + \frac{1}{\bar{g}_V^2} \frac{g_5'^2}{g_5^2} \Pi_V, \quad (107)$$

with $\Pi_{W,A,V}$ as defined in Eq. (97). Recall that all these quantities depend on p^2 , including the \bar{g}_i , even though we do not explicitly indicate so. Expanding in the EWSB masses to the corresponding order in v^2 , one can check that these vacuum polarizations agree exactly with the ones obtained with the method of propagators. Notice, however, that the above formulas hold for arbitrary v . Also, in the limit of UV localized fermions, $c \rightarrow +\infty$, one has $\gamma^{\text{Hol.}} \rightarrow 0$ and $\bar{g}_i \rightarrow 1$, so that Eqs. (106)-(107) reduce to Eqs. (99) and (100).

4. Electroweak Precision Tests

Very precise data from low energy neutrino and electron scattering, LEPI and SLC data at the Z pole, LEPII above the Z pole and the Tevatron impose stringent constraints on any physics beyond the SM [39], commonly called electroweak precision tests (EWPT). These constraints can be computed on each model of new physics by carefully considering the contribution to all the (pseudo)observables that constitute the EWPT. Under the assumption of linearly realized EWSB with a light Higgs and a large enough mass gap with the new physics, one can use the SM effective Lagrangian up to dimension 6 of reference [34] to easily constrain large classes of new models. Not all dimension 6 operators are relevant for EWPT. In general, operators that violate CP or flavour symmetries (except for the third family), operators that only involve quarks or gluons and operators that just renormalize the SM operators (*i.e.* terms of the form $h^\dagger h \mathcal{O}^{\text{SM}}$, with \mathcal{O}^{SM} a dimension 4 operator that is already present in the SM Lagrangian) are irrelevant for EWPT. The relevant ones were classified in Ref. [40] (see also [41]) and their effects on the EWPT computed ([40] gives the χ^2 as a function of

the SM input parameters and the coefficients of the relevant dimension-6 operators). Using the results in Ref. [40] and our calculation of the effective Lagrangian for a general model with custodial symmetry, Eqs. (58) and (62)-(71), one can obtain the constraints in any model of warped extra dimensions with a light Higgs. However, the prototype of realistic warped model, with light fermions localized close to the UV brane, corresponds to universal new physics (except for the third generation) and the corresponding computation of EWPT can be more simply done following [37].

4.1. Tree-level effects

As we discussed in Section 3.1.1, EW precision constraints can be easily implemented in models of universal new physics [37]. In this case, the relevant Lagrangian is given by Eqs. (77) and (79). If we further assume there is a mass gap with the new physics that allows us to reliably expand the vacuum polarizations as

$$\bar{\Pi}(p^2) = \bar{\Pi}(0) + p^2 \bar{\Pi}'(0) + \frac{(p^2)^2}{2} \bar{\Pi}''(0) + \dots, \quad (108)$$

where the prime denotes derivative with respect to p^2 (higher derivative terms give contributions of mass dimension larger than 6), we can parametrize all relevant EWPT in terms of four oblique parameters: †

$$\hat{T} = 1 - \frac{\bar{\Pi}_{33}(0)}{\bar{\Pi}_{+-}(0)}, \quad W = \frac{g^2 M_W^2}{2} \bar{\Pi}_{33}''(0), \quad (109)$$

$$\hat{S} = g^2 \bar{\Pi}_{3B}'(0), \quad Y = \frac{g'^2 M_W^2}{2} \bar{\Pi}_{BB}''(0). \quad (110)$$

Here g , g' and M_W are fixed by the conditions

$$\frac{1}{g^2} = \bar{\Pi}_{11}'(0), \quad \frac{1}{g'^2} = \bar{\Pi}_{BB}'(0), \quad -\frac{M_W^2}{g^2} = \bar{\Pi}_{+-}(0), \quad (111)$$

which, to the order we are interested in, can be identified with the experimentally measured weak gauge couplings and the W mass. Some of these parameters are related to the Peskin-Takeuchi [43] parameters as $\alpha S = 4s_W^2 \hat{S}$ and $\alpha T = \hat{T}$, where α is the electromagnetic fine structure constant.

If EWSB can be treated perturbatively, we can use the general results for the vacuum polarizations (84)-(86) to compute these oblique parameters. For arbitrary v one can use either (93)-(95) for custodially symmetric models with UV localized fermions, or (106)-(107) for models without custodial symmetry, but arbitrary (though universal) fermion localization. In the case that EWSB is a perturbation, the normalization conditions, Eq. (111) give

$$\bar{g}^2 = g^2 [1 - \hat{S}^{\text{Op}}], \quad \bar{g}'^2 = g'^2 \left[1 - \frac{g'^2}{g^2} \hat{S}^{\text{Op}}\right], \quad \bar{v}^2 = v^2 \left[1 + \frac{g^2}{g'^2} \hat{T}^{\text{Op}}\right], \quad (112)$$

† The Z -pole observables plus the W mass depend only on the three linear combinations introduced in [42, 21]. These are $\alpha T_{\text{eff}} = \hat{T} - [W + (s_W^2/c_W^2)Y]$, $\alpha S_{\text{eff}} = 4s_W^2(\hat{S} - W - Y)$ and $\alpha U_{\text{eff}} = 4s_W^2(\hat{U} - W)$ [37].

where \hat{T}^{Op} and \hat{S}^{Op} were defined in Eq. (87). It is then straightforward to check that $\hat{T} = \hat{T}^{\text{Op}}$, $\hat{S} = \hat{S}^{\text{Op}}$ and $W = Y = W^{\text{Op}}$. In the particular case that the fermions are UV localized, and in the absence of custodial symmetry, the oblique parameters are explicitly given by

$$\hat{T}_{UV} = \frac{g'^2}{2g^2}(m_W L_1)^2 \log \frac{L_1}{L_0}, \quad W_{UV} = \frac{(m_W L_1)^2}{4 \log \frac{L_1}{L_0}}, \quad (113)$$

$$\hat{S}_{UV} = \frac{(m_W L_1)^2}{2}, \quad Y_{UV} = \frac{(m_W L_1)^2}{4 \log \frac{L_1}{L_0}}. \quad (114)$$

Note that for UV localized fermions \hat{T} is volume enhanced, \hat{S} is neither enhanced nor suppressed and W and Y are volume suppressed. Thus the most constrained experimentally is \hat{T} , followed by \hat{S} , while W and Y are very mildly constrained. In models with custodial symmetry and UV localized fermions, setting $\alpha \rightarrow \alpha^N - \alpha^D$ as discussed at the end of Subsection 3.2, one finds $\hat{T}_{UV}^{\text{Cust.}} = 0$, so that the most stringent and robust constraints arise from \hat{S} . This is true only for UV localized fermion fields and is not maintained in general for bulk fermion fields.

Light fermions localized on the UV brane are a good approximation in models with a natural realization of flavour. However, the large mass of the top implies that neither of its chirality components can be too far from the IR brane, and in particular that b_L cannot be UV localized. The resulting corrections to the bottom couplings can be computed with identical results using any of the methods we have discussed in Section 2. Here we will use our general result for the effective Lagrangian of models with custodial symmetry, Eq. (58). The part of the effective Lagrangian that we are interested in reads

$$\begin{aligned} \mathcal{L}_{\text{eff}} &= \mathcal{L}_{\text{SM}} + \alpha_{hq}^t \mathcal{O}_{hq}^t + \alpha_{hq}^s \mathcal{O}_{hq}^s + \dots \\ &= \frac{\bar{g}}{2c_W} Z_\mu \bar{b}_L \gamma^\mu b_L \left[-1 + \frac{2s_W^2}{3} - 2v^2(\alpha_{hq}^t + \alpha_{hq}^s) \right] + \dots \end{aligned} \quad (115)$$

Replacing the values of $\alpha_{hq}^{t,s}$ of Eqs. (63) and (64) we obtain for the correction of the $Z\bar{b}_L b_L$ coupling

$$\begin{aligned} \frac{\delta g_{b_L}}{g_{b_L}} &= \frac{2v^2(\alpha_{hq}^t + \alpha_{hq}^s)}{1 - 2s_W^2/3} \\ &= -v^2 \frac{[\bar{g}_L^2 T_L^3 - \bar{g}_R^2 T_R^3] \beta^D + [\bar{g}_L^2 T_L^3 - \bar{g}'^2 Y](\beta^N - \beta_{UV}^N - \beta^D)}{1 - 2s_W^2/3}, \end{aligned} \quad (116)$$

where the quantum numbers and $\beta^{N,D}$ refer to b_L , and we have explicitly subtracted the global effect that we are parameterizing in terms of oblique corrections with the term β_{UV}^N (we are assuming UV localized light fermions). We have separated the correction in two terms. The first term, proportional to β^D , corresponds to the coupling evaluated at zero momentum and, as was the case of \hat{T} , is volume enhanced [see Eq. (73)]. The term proportional to $(\beta^N - \beta_{UV}^N - \beta^D)$ is a correction that arises when the external gauge boson line is evaluated at $p^2 = m_Z^2$, and is neither (volume) enhanced nor suppressed [see (74) and (75)]. This separation is clear if one computes the coupling using the holographic method and the expansion in Eq. (A.9). The volume enhanced term exactly vanishes

if we take either $T_L^3 = T_R^3 = 0$ or $T_L^3 = T_R^3$ and $\bar{g}_L = \bar{g}_R$. The vanishing of the coupling at zero momentum is guaranteed by a subgroup of the custodial symmetry, as first discussed in [16] (and applies to any fermion satisfying $T_R^3 = T_L^3 = 0$ or $T_R^3 = T_L^3$ and $g_L = g_R$). However, the on-shell coupling does not vanish, reading for $T_L^3 = T_R^3$ and $\bar{g}_L = \bar{g}_R$,

$$\frac{\delta g_{b_L}}{g_{b_L}} = -\frac{v^2}{(1 - 2s_W^2/3)} [\bar{g}_L^2 T_L^3 - \bar{g}'^2 Y] (\beta^N - \beta^D - \beta_{UV}^N) . \quad (117)$$

Assuming a boundary Higgs, we obtain using Eqs. (73), (74) and (76),

$$\frac{\delta g_{b_L}}{g_{b_L}} = -\frac{v^2 L_1^2}{4(1 - 2s_W^2/3)} [\bar{g}_L^2 T_L^3 - \bar{g}'^2 Y] [g_2(c_{b_L}) - 2\tilde{g}_2(c_{b_L})] . \quad (118)$$

where $g_2(c)$ and $\tilde{g}_2(c)$ are defined in Eqs. (A.7) and (A.8) of the appendix.

4.2. Loop effects

So far we have concentrated on tree-level effects. Due to the summation over the KK towers, loop effects can generically be expected to be relevant. In generic theories such effects are usually UV sensitive and can only be estimated, e.g. based on NDA in higher dimensions [44]. However, in theories with custodial symmetry [15] (and custodial protection of some fermion couplings to the Z [16]) some of the EW (pseudo)observables, namely T and δg_{b_L} , are calculable, since the symmetries forbid the associated counterterms. It is therefore pertinent to assess more carefully the importance of such effects. The one-loop contribution to the T -parameter due to the top KK tower was computed in certain scenarios in [45] (see also [46]). For instance, when the fermions are assigned to representations that protect the contributions to δg_{b_L} , it was found that typically the effect of the top sector on T decreases with respect to the SM (i.e. the massive KK tower gives a *negative* ΔT). This can select rather well-defined regions of parameter space. The contributions due to gauge loops have not been computed. Also, the one-loop contributions to δg_{b_L} were computed in [9]. These tend to be small, but not necessarily negligible. As we will see in the next section, such loop contributions can be important in relaxing the constraints from EW precision measurements on the scenarios we consider.

4.3. Summary of EW constraints in models with custodial symmetry

With the low-energy effective Lagrangian presented in the previous sections one can assess the indirect constraints from precision measurements on models with custodial symmetry in warped spaces, under the assumption that there exists a light Higgs degree of freedom. In the general case that the fermions propagate in the bulk, one should perform a global fit to the EW observables based on the dimension-6 Lagrangian of Eq. (58). Such an analysis was performed in [9]. It was found that, depending on the SM fermion $SU(2)_R$ quantum number assignments, the bounds from the EW constraints on

the gauge boson masses are typically in the 2.5-3.5 TeV range (neglecting brane kinetic terms), although in certain models they could be as low as 1.5 TeV.

Due to the T_R^3 charges in Eqs. (64) and (66), the low-energy effects of the heavy physics are in general not universal, even when all fermions share the same localization profiles. However, the RS interpretation of the flavor structure as arising from “anarchy” of the Yukawa couplings (see Section 5 below) requires that the light fermion families be localized close to the UV brane, in which case the low-energy corrections become of the universal type (the effects of the massive $SU(2)_R$ gauge bosons become exponentially suppressed and the c -dependence of Eqs. (68) and (69) disappears). It is then simpler to use the fits based on the oblique parameters, Eqs. (109) and (110). The dependence on the model parameters is given in Eq. (87). Furthermore, for UV localized fermions, W and Y are volume suppressed and can be neglected. However, in general the corrections to the $Z\bar{b}_L b_L$ coupling, which at tree-level are given by Eq. (116), need to be taken into account. When $g_L = g_R$ and $T_L^3 = T_R^3$ the tree-level contributions to δg_{b_L} are relatively small due to a custodial protection [16], but there can be non-negligible loop-level effects. Thus, a fit to S , T and δg_{b_L} is typically appropriate.

Using the code of Ref. [40], we obtain the 1σ ($\Delta\chi^2 = 1$) intervals

$$S = -0.03 \pm 0.09, \quad T = 0.03 \pm 0.09, \quad \frac{\delta g_{b_L}}{g_{b_L}} = (-0.4 \pm 1.4) \times 10^{-3}. \quad (119)$$

Here we have used the combined CDF and DØ top mass measurement of March-2009 (using up to 3.6 fb^{-1} of data per experiment): $m_t = 173 \pm 1.3 \text{ GeV}/c^2$ [47], as well as the combined CDF/DØ W mass measurement of Aug.-2008: $M_W = 80.432 \pm 0.039 \text{ GeV}/c^2$ [48]. We include the Z -pole observables, the low-energy measurements (except for NuTeV), and LEP II data. We also used a Higgs mass of $m_{h_{\text{ref.}}} = 117 \text{ GeV}$.

In models without custodial protection the main constraint comes from $T = \alpha \hat{T}$. Requiring $T^{\text{tree}} < 0.21$ (at 2σ), assuming a light Higgs as in the fit of Eq. (119), and using Eq. (113), gives a strong lower bound of $1/L_1 \sim 4.4 \text{ TeV}$ (hence gauge boson masses $M_{\text{KK}} > 2.45/L_1 \approx 11 \text{ TeV}$). Such a constraint can be somewhat relaxed for a heavier Higgs (and for sizable gauge and/or fermion brane kinetic terms [21]). The situation is dramatically improved in models with custodial protection, since T^{tree} vanishes in this case (for UV localized fermions). A bound based on $S < 0.15$ (at 2σ) alone results in $1/L_1 \sim 1.5 \text{ TeV}$ ($M_{\text{KK}} > 3.7 \text{ TeV}$). However, falling inside the 95% C.L. ellipsoid ($\Delta\chi^2 = 7.81$ for three parameters: S , T and δg_{b_L}) can allow for $S \sim 0.23$ (if $T \sim 0.25$ and $\delta g_{b_L}/g_{b_L} \sim -0.8 \times 10^{-3}$). In this case, and in the absence of additional contributions to S , one can have $1/L_1 \sim 1.25 \text{ TeV}$ ($M_{\text{KK}} > 3 \text{ TeV}$). As mentioned in the previous subsection, loop level contributions to T and δg_{b_L} can be relevant (and depend on additional model parameters, although typically ΔT^{loop} and $\delta g_{b_L}^{\text{loop}}$ are correlated). Requiring that these additional contributions optimize the EW fit usually selects well-defined regions of parameter space (e.g. localization of the third family quarks).

In conclusion, we see that models with custodial protection and an implementation of the flavor structure through fermion localization can be consistent with gauge boson KK excitation of about 3 TeV. These could be somewhat lighter in the presence of

moderate IR brane kinetic terms. Also, playing with the localization parameters of LH versus RH fermions it may be possible to lower this scale somewhat more. Another possibility compatible with a lower scale of new physics is to consider a different background, e.g. soft-wall models (see for instance [49]-[53]). We will take these scales as a guide to the study of the collider phenomenology, to be undertaken in the second part of this review.

Higgsless models [19], which have not been covered in this review due to lack of space, require a much lower scale that can be made compatible with EWPT at tree level by localizing the light fermions close to $c = 1/2$ [54] for which all corrections become small, and imposing the custodial protection of the T parameter and the $Z\bar{b}b$ coupling [55] (for a review, see [56] or Section 3 of [57]).

5. A few remarks on flavour (constraints)

As remarked in the introduction, the RS framework with bulk fields provides a theory of flavor. The main idea [7] arises from the c -dependence of the fermion zero-mode wavefunctions (18): for $c > 1/2$, the profiles are localized near the UV brane and therefore the overlap with an IR localized Higgs field (so as to address the hierarchy problem) is exponentially suppressed. This allows one to easily generate hierarchical effective 4D Yukawa couplings, even if the microscopic 5D Yukawa couplings exhibit no special structure, an assumption usually called “anarchy” (in other scenarios, such as gauge-Higgs unification, the fermion-Higgs interactions depend on localized fermion mixing mass parameters to which the anarchy assumption can be applied). In warped spaces, with their associated z -dependence of the cutoff scale, (light) fermion localization near the UV brane also provides an effective cutoff on non-renormalizable flavour-violating operators that is sufficiently high to significantly suppress their effects, even with the new KK physics entering at a few TeV.

The consequences of “anarchy” for flavour physics were considered originally in [10]-[14] and more recently in [58]-[66]. The largest effects arise at tree-level from flavour changing KK gluon couplings. Although most of the predictions are consistent with current flavour constraints for the scales determined by the EWPT –and often lead to interesting expectations for indirectly observing the new physics in the near future– there are some observables that can impose more severe bounds. Most notably CP violation in the kaon system can lead to a bound of $\mathcal{O}(10)$ TeV on the KK scale [58].

Thus, a strict application of the anarchy assumption can result in a KK scale beyond the reach of the LHC. This may suggest that flavour symmetries are at work, see e.g. [67]-[75], or perhaps that these models exhibit a moderate amount of fine-tuning (hopefully in the flavour sector, so that discovering the new physics at the LHC remains a possibility). Given the model dependence of such conclusions, we will take the more robust bounds from EW precision measurements as a starting point to summarize the

LHC collider phenomenology of warped scenarios.

Part II Collider Phenomenology of Warped Models

Contributed by H. Davoudiasl and S. Gopalakrishna

In our presentation of the collider phenomenology of warped models, we will use a different notation from that of the preceding discussion. This is largely done to match the conventions used in several of the papers that are cited in the following review. In our notation, $k = 1/L_0$ and the size of the extra dimension is denoted by πr_c . Also, note that, in most of what follows, the LHC center of mass energy $\sqrt{s} = 14$ TeV is assumed, unless otherwise specified. Obviously, given the parton distribution function (PDF) dependence of cross sections for production of TeV-scale KK modes, many of the conclusions presented below have to be revisited for smaller values of \sqrt{s} .

6. KK Gravitons

We begin our discussion of KK phenomenology with the graviton sector, since KK gravitons were the first tower of states whose collider phenomenology was studied [3] and constitute a key and common signature of warped models. As noted previously, in the original RS model the entire SM content was assumed to be confined to the IR-brane. The most distinct signature of this setup was then the tower of graviton KK modes. These states would appear as a series of spin-2 resonances close to the weak scale, which sets the scale of their masses and couplings to the SM. Specifically, the KK graviton masses are given by

$$m_n^G = x_n^G k e^{-kr_c\pi}, \quad (120)$$

where $x_n = 3.83, 7.02, \dots$, for $n = 1, 2, \dots$, are given by the roots of J_1 Bessel function, to a very good approximation [3]; the zero mode for ($n = 0$) is the massless 4D graviton. The interactions of the graviton KK modes with the SM fields are given by

$$\mathcal{L} = -\frac{1}{\bar{M}_P} T^{\alpha\beta}(x) h_{\alpha\beta}^{(0)}(x) - \frac{1}{\Lambda_\pi} T^{\alpha\beta}(x) \sum_{n=1}^{\infty} h_{\alpha\beta}^{(n)}(x), \quad (121)$$

with $\bar{M}_P \sim 10^{18}$ GeV the reduced Planck mass, $T_{\alpha\beta}$ the SM energy-momentum tensor, $h_{\alpha\beta}^{(n)}(x)$ KK modes of the graviton, and $\Lambda_\pi \equiv e^{-kr_c\pi} \bar{M}_P$ [3].

The best direct limits on the original RS model are from the Tevatron experiments. We present recent limits from the CDF [76] and D0 [77] experiments in Figs. 2 and 3. The graviton KK phenomenology of the original RS model can be described by the KK mass and the ratio k/\bar{M}_P . Calculations in this background are reliable as long as k/M_5 is not $\mathcal{O}(1)$ or larger (this is a classical argument that can be somewhat modified if we consider quantum effects [78]). For this reason, $k/\bar{M}_P \lesssim 1$ is often considered in phenomenological and experimental studies, as seen for example in these figures. We see

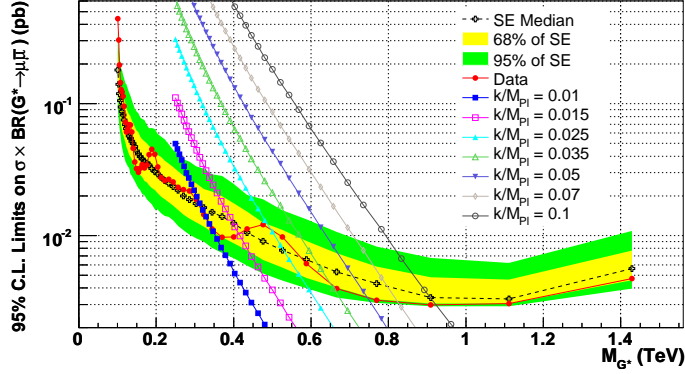


Figure 2. CDF limits (95% confidence level) [76] on the product of cross section and dimuon branching fraction, for the lightest KK graviton in the original RS model. Theoretical cross sections and expected limits from simulated experiments (SE) are also shown.

that the direct bounds on the mass of the lightest KK graviton range over 300-900 GeV for $0.01 \leq k/\bar{M}_P \leq 0.1$. The LHC reach for the first graviton KK mode in this model has been calculated by ATLAS [79] and CMS [80] collaborations and is roughly 3.5 TeV with 100 fb^{-1} of integrated luminosity.

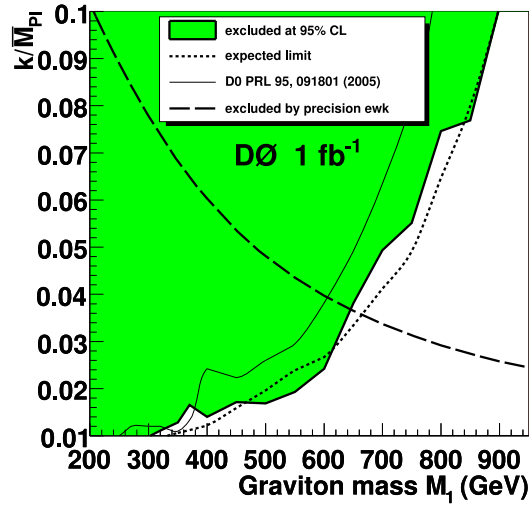


Figure 3. D0 bounds [77] on the lightest KK graviton mass, as a function of k/\bar{M}_P , in the original RS model.

Once we extend the RS setup to provide a model of flavor, the above conclusions regarding the graviton KK phenomenology at colliders change drastically. The current Tevatron bounds do not take these effects into account, however we generally expect the direct bounds to become much weaker. This is due to the fact that, in warped flavor models, KK graviton couplings to UV-localized light fermions get highly suppressed [81] roughly like their Yukawa couplings [78], and couplings to gauge fields (in units of $1/\bar{M}_P$)

[81]

$$C_{00n}^{AAG} = e^{kr_c\pi} \frac{2 [1 - J_0(x_n^G)]}{kr_c\pi (x_n^G)^2 |J_2(x_n^G)|}, \quad (122)$$

where $J_{0,2}$ denote Bessel functions, get volume $(kr_c\pi)$ suppressed. Hence, as alluded to before, important production and decay channels become either inaccessible or else suppressed. Given that a TeV-scale graviton KK tower is the most generic prediction of the RS model, largely independent of various model building assumptions, it is worth reconsidering its phenomenology within warped flavor models.

The reach of the LHC experiments for the lightest graviton KK mode was accordingly reexamined in Refs. [82] and [78]. With the light fermions basically decoupled, the dominant production channel at the LHC is through gluon fusion, which is suppressed by $(kr_c\pi)^{-1}$. As for the dominant decay channels, generically we expect the right-handed top t_R and the Higgs sector, including the longitudinal gauge fields Z_L and W_L^\pm , to be the only important final states, due to their large overlap with the graviton KK wavefunction \ddagger . With these assumptions, the partial widths of the first KK graviton into pairs of t_R , the Higgs boson h , Z_L , and W_L^\pm are given, respectively by [82, 78]

$$\frac{\Gamma_{t_R}}{3N_c} = \Gamma_h = \Gamma_{Z_L} = \frac{\Gamma_{W_L}}{2} = \frac{(\bar{c} x_1^G)^2 m_1^G}{960\pi}, \quad (123)$$

where $N_c = 3$ is the number of colors in QCD, $\bar{c} \equiv k/\bar{M}_P$ (our barred notation for this parameter differs from that of Ref. [78], to avoid confusion with the bulk fermion mass parameter c , discussed before), and final states have been treated as massless, which is a good approximation due to the much larger expected mass of the KK mode. Also, the decay widths to longitudinal polarizations have been estimated using the equivalence theorem [which is valid up to $M_{W,Z}^2/(m_1^G)^2$ corrections] to relate these widths to that of the physical Higgs. Here, we note that two-body decay into final states that include a KK mode and a heavy SM mode are either (i) volume suppressed, when the relevant zero mode has an approximately flat profile, or (ii) kinematically forbidden (due to a large KK fermion mass), or else (iii) suppressed by a power of $\langle H \rangle$. If we assume that t_R is highly IR-brane-localized (ii) applies to an otherwise potentially important $G_1 \rightarrow \bar{t}_R t_{R1}$.

Given the above considerations, Ref. [82] focused on the $t_R \bar{t}_R$ final state to estimate the LHC reach for the lightest KK graviton. One of the issues that affects the utility of this channel is the efficiency for top identification, made more challenging because of the collimated decay products of highly boosted tops. We will discuss this issue in greater detail in later sections. The narrow width of the KK graviton, under the above assumptions, can be helpful in limiting the background in this channel. However, one has to account for smearing of the measured resonance mass.

\ddagger Quite often (however not as a rule [45]), it is the right-handed top quark that is the most IR-localized SM fermion, given that the doublet $(t, b)_L$ is subject to precision bounds on b -quark couplings, as noted in the preceding discussion of precision constraints.

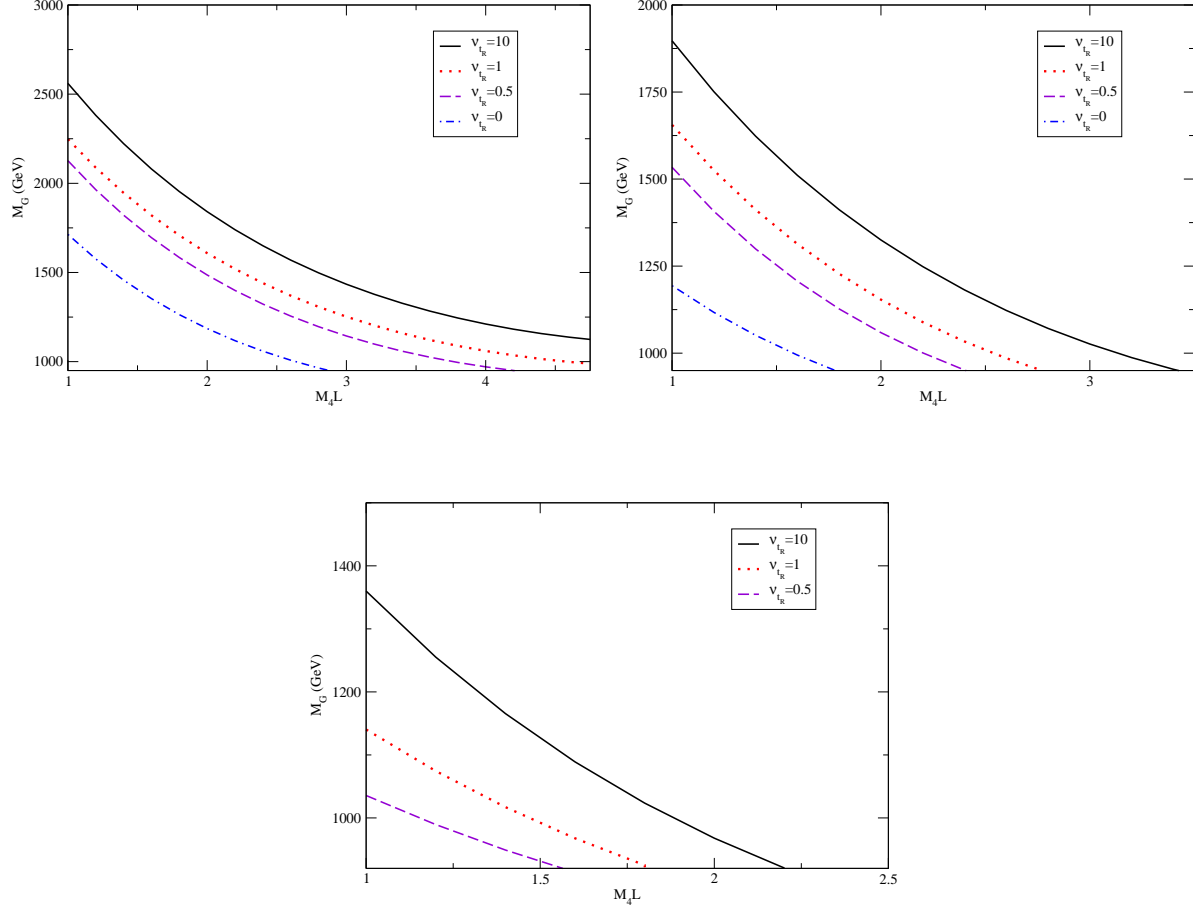


Figure 4. The reach ($S/\sqrt{B} = 5$) for the lightest KK graviton G_1 , from Ref. [82], with 100 fb^{-1} of integrated luminosity and top identification efficiency 100%, 10%, and 1%, clockwise from the top. With increasing ν_{t_R} (corresponding to $-c_{t_R}$ in the notation of Part I) the profile of t_R is more IR-localized; M_4L corresponds to $1/\bar{c}$ in our notation.

In Ref. [82], the background was taken to be all $t\bar{t}$ with invariant mass within 3% of m_1^G , corresponding to a typical smearing $E \times 3\%$ for the ATLAS experiment. The top identification efficiency was treated as uncertain in this work and the reach, given by $S/\sqrt{B} = 5$, assuming 100 fb^{-1} of integrated luminosity, was considered for three values of efficiency, 1%, 10%, and 100%, as presented in Fig. 4. These results suggest that the reach for G_1 may be expected to be 1.5-2 TeV, depending on top identification efficiency.

Given that the longitudinal gauge bosons Z_L and W_L^\pm are manifestations of the IR-localized Higgs sector Goldstone modes, their couplings to the graviton KK modes are substantial, as deduced from Eq. (123). In particular, the process $pp \rightarrow G_1 \rightarrow Z_L Z_L$ with both Z 's decaying into $\ell^\pm = e^\pm, \mu^\pm$, provides a clean signal, unencumbered by complicated event reconstructions. In the absence of prompt di-lepton and di-photon channels, this process provides a “golden mode” for KK graviton discovery. Based on

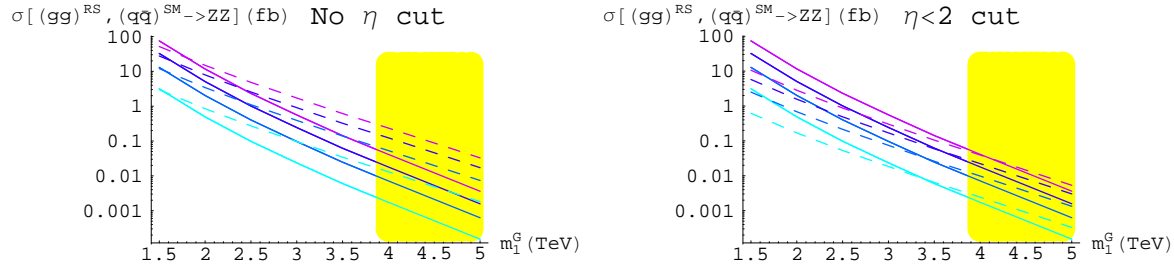


Figure 5. The cross-sections (integrated over one width) for $gg \rightarrow ZZ$ via KK graviton (solid lines) and the corresponding SM background (dashed lines), for $\bar{c} = 0.5, 1, 1.5, 2$ (from bottom to top), with no cut on η (left panel) and $\eta < 2$ (right panel). The yellow region shows the expected KK graviton mass in the simplest models based on gauge KK mass from precision tests [78].

these considerations, Ref. [78] examined the possibility of searching for warped gravitons in the $Z_L Z_L$ decay channel.

In Ref. [78], it was determined that the vector boson fusion cross section for KK graviton production is roughly an order of magnitude smaller than the gluon fusion channel considered above. The dominant SM background to ZZ production though comes from $q\bar{q}$ initial states. Hence, one expects forward-backward cuts on pseudo-rapidity η to be efficient in reducing the background, mediated via t/u channels, while not affecting the signal a great deal; this was shown to be case in Ref. [78], typically yielding S/B significantly larger than unity. Note that due to negligible initial state $q\bar{q}$ coupling to G_1 , the signal and background do not interfere to a good approximation.

The reducible SM background to the above KK graviton signal depends on the decay modes of the Z 's. For hadronic decays of both Z 's, the 4 jet QCD background was deemed too large to allow this channel to be of use. Even the case with one Z decaying hadronically and the other decaying into ℓ^\pm poses a serious challenge. This is due to the large boost of the Z 's (similar to t 's in the previous discussion) which makes the opening angle of signal di-jets of order $M_Z/\text{TeV} \sim 0.1$ [78] while typical cone size for jet reconstruction was taken to be $\mathcal{O}(0.4)$ (as quoted from Ref. [83]). This makes the relevant SM background to come from $Z + j$, which was calculated to be an order of magnitude larger over the resonance width. This problem of jet-merging in the decays of highly boosted particles is a generic challenge in searches for TeV scale resonances that preferentially decay into heavy SM final states, and will be encountered in our later discussions of other KK modes.

Based on the clean 4ℓ final state, the signal and background were calculated over the KK graviton width Γ_G , as shown in Fig. 5. We can see from the plots that the η -cut significantly improves S/B ; the dependence of background on \bar{c} comes from the dependence $\Gamma_G \propto \bar{c}^2$ that sets the integration interval. Naive dimensional analysis suggests that higher curvature terms are suppressed by $\Lambda \sim 24^{1/3} \pi M_5$ [78], which is

why values of $\bar{c} > 1$ were considered. Ref. [78] concluded that for $\bar{c} \lesssim 2$ (for reliable calculations), the LHC reach ($S/\sqrt{B} > 4$) for G_1 is about 2 (3) TeV with 300 (3000) fb^{-1} .

Another potentially important channel for KK graviton discovery is via the $W_L^+ W_L^-$ final state, discussed in Ref. [84]. These authors note that the KK graviton has a branching fraction into the W_L^\pm twice that for the $Z_L Z_L$ final state and that the branching fraction of the W^\pm into a leptonic final state is about 11% compared to 3% for the Z . However, when the highly boosted W 's decay into leptons, the neutrinos will be mostly back-to-back and the missing energy information will be lost [78, 84]. In addition, the hadronic decay of one of the W 's will again be collimated and be subject to a large $W + j$ background [78, 84]. The results of Ref. [84] suggest that the reach for the KK graviton in the W_L^\pm channel with 300 fb^{-1} will not be significantly above 2 TeV, unless analysis techniques are developed to suppress the $W + j$ background.

In case a graviton KK mode is detected at the LHC, it would be important to establish its spin. Ref. [85] considered whether this is feasible and concluded that, with 1000 fb^{-1} , the KK graviton spin for masses up to ~ 2 TeV may be confirmed. Ref. [86] also considered this question, but in the original model RS model with the entire SM on the IR brane, where e^\pm and μ^\pm decay modes are accessible. These authors found it feasible for masses of ~ 1 TeV to establish the KK graviton spin. However, we again note that the original RS model is subject to stringent bounds on cutoff-scale operators which, in the absence of tuning, would require $m_1^G \gg 1$ TeV.

Simple warped models predict that the lightest graviton is $3.83/2.45 \simeq 1.56$ times heavier than the lightest KK gauge boson. Given the preceding discussion of precision data, it is then expected that $m_1^G \gtrsim 4$ TeV, corresponding to the yellow regions in Fig. 5. Therefore, the above analyses suggest that, in generic models, discovering the warped KK graviton at the LHC is quite challenging, at design or perhaps even upgraded (SLHC [87, 88]) luminosity.

7. KK Gluons

The KK gluons g_n generally offer the best reach for discovery at the LHC, as indicated by the results of Refs. [89] and [90] that we summarize below; we will not present the details of the analysis in these works and refer the interested reader to these references for more information. First of all, the level-1 KK gauge fields are generally expected to be the lightest such excitations, within the known (SM \oplus gravity) sectors; the KK masses for a gauge field A are given by Eq. (120) with $x_n^G \rightarrow x_n^A \simeq 2.45, 5.57, \dots$. Secondly, the $SU(3)_c$ coupling constant g_s of the SM gluon is larger than those of other SM gauge fields. This leads to a larger production cross section, which is proportional to g_s^2 , for the KK gluons. However, in realistic models of flavor, the couplings of g_1 to light flavors are diminished compared to its SM counterpart (g_0 , the gluon), suppressing production through light quarks at colliders; the couplings to the gluon of the SM are zero by orthonormality of KK modes. On the other hand, the dominant branching fraction is set by coupling to IR-localized top quarks, which is enhanced compared to the SM

gauge coupling. This leads to a large width for KK gluons $\Gamma_g \sim m_1^g/6$ for $m_1^g \gtrsim 1$ TeV (demanded by precision data), and renders the extraction of a discovery signal more difficult.

The work of Ref. [89] focused on a setup in which $Q^3 = (t, b)_L$ was quasi IR-localized, t_R was basically on the IR-brane, and all other fermions f were UV-localized. Let $\xi \equiv \sqrt{\log(\bar{M}_P/\text{TeV})} \approx \sqrt{kr_c\pi} \sim 5$. Then the couplings of the lightest KK gauge field $A^{(1)}$ are given by the following approximate relations [89]

$$\frac{g_{f\bar{f}A^{(1)}}}{g_{\text{SM}}} \simeq 1/\xi; \quad \frac{g_{Q^3\bar{Q}^3A^{(1)}}}{g_{\text{SM}}} \approx 1; \quad \frac{g_{t_R\bar{t}_RA^{(1)}}}{g_{\text{SM}}} \simeq \xi; \quad \frac{g_{A^{(0)}A^{(0)}A^{(1)}}}{g_{\text{SM}}} \approx 0; \quad \frac{g_{HHA^{(1)}}}{g_{\text{SM}}} \simeq \xi \quad (124)$$

where g_{SM} denotes a generic SM gauge coupling, $A^{(0)}$ is a gauge field zero mode. Note that H includes both the physical Higgs (h) and *unphysical* Higgs, i.e., *longitudinal* W/Z by the equivalence theorem (the derivative involved in this coupling is similar for RS and SM cases and hence is not shown for simplicity). For the case of KK gluons, the last coupling in Eq.(124) does not exist and the fourth equality is exact, since $SU(3)_c$ is unbroken. Here, the effects of EWSB, expected to be small, are ignored. We note that, in alternative models that possess a custodial symmetry to protect the coupling $Zb\bar{b}$, one can arrange for the couplings of Q^3 and t_R to be interchanged or for both to have intermediate values [16].

At the LHC, the dominant g_1 production is through the $u\bar{u}$ and $d\bar{d}$ initial states. However, the background $t\bar{t}$ is mainly from gg fusion and more forward-peaked. Hence, a p_T cut suppresses the background more than the signal. In Ref. [89], the preferred reconstruction mode was $t\bar{t} \rightarrow b\bar{b}jj\ell\nu$. In order to minimize the impact of parton distribution function (PDF) uncertainties, this work focused on the differential cross section as a function of the $t\bar{t}$ invariant mass $m_{t\bar{t}}$ and looked for a “bump” in this distribution; due to the large width of the KK gluon a sharp resonance is not expected. Particle and parton level results from Ref. [89] are shown in the left panel of Fig. 6. With a total efficiency of order 1%, including b -jet-tagging (20%) and cut (about 20%) efficiencies, as well as the branching fraction to the final state (0.3), it was concluded that $S/\sqrt{B} = 11.0(4.2)$ and $S/B = 2.0(1.6)$ for $m_1^g = 3(4)$ TeV are achievable for 100 fb^{-1} , at the LHC [89]. It is then concluded that the LHC reach for the KK gluon g_1 is $m_1^g \lesssim 4$ TeV.

It is also noted in Ref. [89] that the enhanced coupling of t_R (in this setup) to KK gluons provides an important handle on the signal, since, whereas in the warped model the decay of the KK mode is largely dominated by t_R , the SM background is dominated by QCD which is left-right symmetric. Here, due to the large boost of the top quark, its chirality is preserved and can be deduced from its decay products: leptons tend to be forward (backward)-emitted, in the rest frame of $t_{R(L)}$, relative to the direction of the top quark boost. Defining

$$P_{LR} = 2 \times \frac{N_+ - N_-}{N_+ + N_-}, \quad (125)$$

where N_{\pm} is the number of forward/backward positrons in the above sense, the right panel of Fig. 6 shows a distinct asymmetry which can be correlated with bumps in

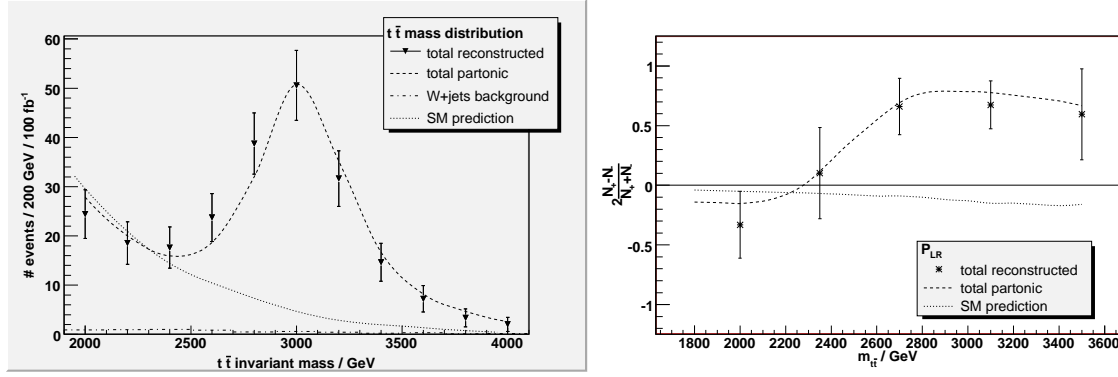


Figure 6. Left panel: Invariant $t\bar{t}$ mass distribution (left panel) and P_{LR} (right panel). In both panels $m_1^g = 3$ TeV, for parton-level signal+background (dashed) and SM prediction (dotted); the Wjj background is also shown (dashed-dotted) in the left panel. The error bars correspond to the statistical uncertainties in the particle-level analysis. These plots are from Ref. [89].

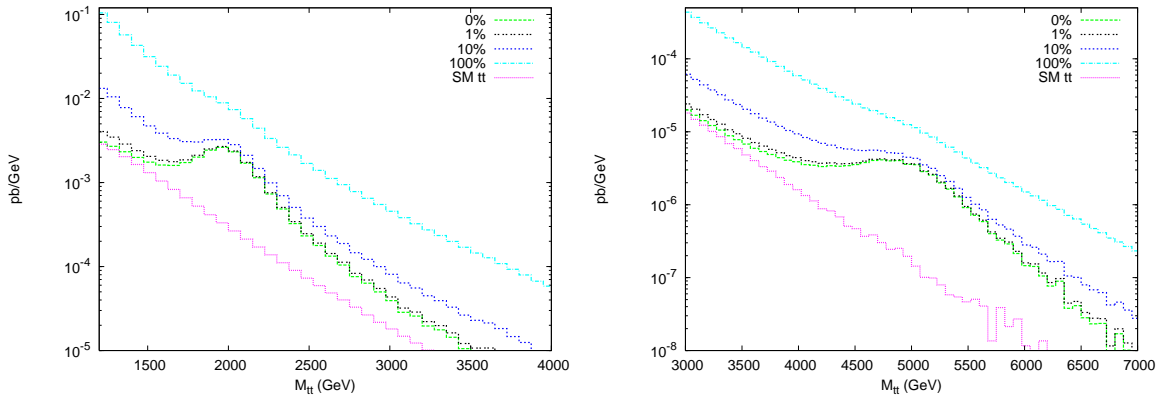


Figure 7. $t\bar{t}$ invariant mass distribution for signal plus some background, given different values of the top-tagging fake rate, for $m_1^g = 2(5)$ TeV in the left (right) panel.

the invariant mass distribution. Note that in the above setup, the much smaller SM asymmetry, mostly from the left-handed weak coupling, has the opposite sign in the signal region [89].

An independent study regarding the LHC reach for g_1 was performed in Ref. [90], using assumptions about the fermions profiles similar to that discussed above. This resulted in nearly the same level of suppression in the production, dominance of the t_R branching fraction, and total width. Here, as in Ref. [89], it was recognized that, for reasonable values of m_1^g , the highly boosted final state tops will have collimated decay products. Hence, the usual techniques of top identification will not be applicable and new methods have to be developed to gain control over the background.

In Ref. [90], the effects of potential methods for background suppression, generally requiring a detailed knowledge of jet morphology and detector simulations, were parametrized by a range of signal dilution factors. In Fig. 7, the $t\bar{t}$ mass distribution for

$m_1^g = 2$ (5) TeV is presented in the left (right) panel. Here, the two-object $t\bar{t}$ final states are subject to QCD di-jets and $b\bar{b}$ backgrounds that fake the signal. The various curves in each panel represent different levels of fake rate and suggest that signal extraction is possible if a background rejection factor of about 10 is achieved. Ref. [90] concludes that based on their analysis, given 100 fb^{-1} , a conservative LHC reach for g_1 is about 5 TeV. Note that this is a somewhat more optimistic conclusion than that reached above. The authors of Ref. [90] attribute this to the different method, based on strong cuts, adopted in Ref. [89] to identify hadronic tops that could result in a more limited reach. Here, we note that without a more detailed study based on jet structure and realistic simulations of background rejection, it is difficult to determine how conservative this extended reach is. In any case, given that realistic values of KK gluon mass lie above 2-3 TeV, we see that in either case, the LHC can potentially access interesting values of m_1^g . Identifying boosted tops are also studied in Refs. [91, 92].

The spin of the KK gluon provides another handle on the signal. The prospects for establishing the $1 + \cos^2 \theta$ behavior of the signal top angular distribution was examined in Ref. [90]. While this distribution has a characteristic forward-peaked structure, the background is also strongly forward-peaked. Strong p_T cuts on reconstructed tops or tagged top-jets could largely suppress the background and enhance S/B . However, we note that a good grasp of top-tagging efficiency and background rejection is needed before a firm conclusion can be made. This work also considered the possibility of establishing the chiral structure of the gluon KK coupling, in a fashion similar to that of the preceding discussion, concluding that it is feasible to do so for m_1^g up to 2-3 TeV, above which lepton isolation cannot be effectively achieved, making the requisite measurements more challenging.

Ref. [93] considers $t\bar{t}$ final state resulting from the production of the gauge KK's. The observables are dominated by the KK gluon since its cross section is much bigger than the EW KK's. Similar to Ref. [89] they show that the forward-backward asymmetry of the top-quark can be significantly altered from the SM prediction. Moreover, Ref. [94] explains the 2σ deviation in the $t\bar{t}$ forward-backward asymmetry at the Tevatron by a 3 TeV KK gluon contribution, while the long-standing 3σ discrepancy in the b -quark forward-backward asymmetry is improved by the EW gauge KK contributions [95].

Associated production: Refs. [96] and [93] consider the associated production of the KK gluon with either $t\bar{t}$ or $b\bar{b}$, with the KK gluon decaying to $t\bar{t}$. Taking into account irreducible backgrounds, they find that the reach at the LHC with 100 fb^{-1} is about 3 TeV in this channel. They point out that optimizing the cuts might lead to a better reach, although dealing with combinatorics for the 4-top final-state is no trivial matter.

Before closing this section, we note that, during initial phases, the LHC may operate at or below $\sqrt{s} = 10$ TeV. Given that the KK gluon is a promising mode of discovery for warped scenarios, here we would like to provide an estimate of the LHC reach for this state at the lower center of mass energy. As a check of our estimate, first we consider the reach at $\sqrt{s} = 14$ TeV. Consistent with the aforementioned results of Ref. [89], we find for $m_1^g = 3$ TeV that the luminosity required at the LHC for a 5σ significance at

$\sqrt{s} = 14$ TeV is about 25 fb^{-1} , for cuts and efficiencies given therein. For $\sqrt{s} = 10$ TeV, using a Monte Carlo simulation, we find that the luminosity required for 5σ discovery increases to about 115 fb^{-1} , for similar cuts and efficiencies.

8. Electroweak KK states (KK W and Z)

We restrict our discussion here to models where the electroweak gauge group in the bulk is taken to be $SU(2)_L \otimes SU(2)_R \otimes U(1)_X$, with hypercharge being a linear combination of $U(1)_R$ and $U(1)_X$. The extra $SU(2)_R$ (relative to the SM) ensures suppression of the contributions to the EWPT (especially the T parameter) [15]. The detailed theory and LHC phenomenology of the neutral EW states are presented in Ref. [97], and that of the charged EW states in Ref. [98] from which we will summarize the main aspects of their results. For just the SM gauge group in the bulk, see Ref. [99] for a discussion of the AdS/CFT correspondence and LHC signatures.

In these theories, there are three neutral electroweak gauge bosons denoted as W_L^3 , W_R^3 and X , and two charged gauge bosons denoted as W_L^\pm and W_R^\pm . The $SU(2)_R \otimes U(1)_X \rightarrow U(1)_Y$ symmetry breaking by b.c.'s leaves one combination of zero-modes in (W_R^3, X) massless (the hypercharge gauge boson B) while rendering the orthogonal combination (Z_X) massive. In the charged sector this breaking leaves the W_R^\pm without a zero-mode. The SM Higgs doublet is promoted to a bi-doublet of $SU(2)_L \otimes SU(2)_R$ with zero $U(1)_X$ charge and like in the SM, is responsible for $SU(2)_L \otimes U(1)_Y \rightarrow U(1)_{EM}$ symmetry breaking by the Higgs VEV. This leaves one combination of zero-modes in (W_L^3, B) massless (the photon A), while making massive the orthogonal combination (Z), and in the charged sector making the W_L^\pm massive.

The bulk gauge fields can be expanded as a tower of KK states. In each of these neutral and charged tower of states, we will restrict to the zero and 1st KK modes only. The zero-mode is the SM, and we will denote the 1st level KK neutral states by A_1 , Z_1 and Z_{X1} , and the charged ones by W_{L1}^\pm and W_{R1}^\pm .

EWSB mixes these states and the resulting mass eigenstates are denoted by the neutral \tilde{A}_1 , \tilde{Z}_1 and \tilde{Z}_{X1} , and the charged \tilde{W}_{L1} , \tilde{W}_{R1} . We will also collectively refer to the heavy neutral mass eigenstates as Z' , and the charged ones as W' . Note that the (EW preserving) KK masses for the first KK states (for both the neutral and charged KK states) are quite degenerate such that the EWSB mixing (mass)² term is larger than KK (mass)² splitting for $m_{KK} \lesssim 3.5$ TeV. Hence, for the interesting range of KK masses, we expect large mixing between Z_1 and Z_{X1} in the neutral sector (the A_1 does not mix), with the heavy mass eigenstates roughly 50 – 50 admixtures of Z_1 and Z_{X1} and a small admixture of $Z^{(0)}$. The lightest mass eigenstate is of course identified as the SM Z boson and is mostly the $Z^{(0)}$. Similarly in the charged sector, the two heavy mass eigenstates are a large mixture of $W_R^{(1)+}$ and $W_L^{(1)+}$ with a small admixture of $W^{(0)+}$. Although the mixings between the first and zero levels are small, it is important to keep these effects in Z' and W' decays to SM gauge bosons, since they lead to $O(1)$ effects when the small mixings are overcome by the enhancement due to the longitudinal polarization of the

energetic Z and W in the final state (as expected from the equivalence theorem).

Couplings: As already mentioned, warped models can naturally explain the SM fermion mass hierarchy. In such models, as shown schematically in Eq. (124) ignoring small EWSB effects, the light SM fermions have a small couplings to all KK's (including graviton) based simply on the overlaps of the corresponding profiles, while the top quark and Higgs have a large coupling to the KK's. The exact couplings including EWSB effects are presented in Refs. [97, 98].

Phenomenology: Here we summarize the main results of Refs. [97] and [98] that studied the KK Z and W comprehensively. The results presented below are for the following choices of fermion bulk mass parameters: $c_{Q_L^3} = 0.4$, $c_{t_R} = 0$, and all the other c 's > 0.5 , and for $\xi = \sqrt{k\pi r_c} = 5.83$. The $Zb\bar{b}$ coupling can be protected [16] against excessive corrections by making the third generation quarks bidoublets under $SU(2)_L \otimes SU(2)_R$ by including extra non-SM fermions to complete the representation. The W' can decay to some of these extra non-SM fermions which is taken into account in computing the BRs in Ref. [98], but as a first-step the analysis is based on SM final states only.

The total width of the KK Z and W are typically about 5 to 10 % of their mass. For reasons already mentioned, they predominantly decay into heavier fermions (top), and to the Higgs (including W_L and Z_L , the longitudinal modes). The main decay channels are: $Z' \rightarrow t\bar{t}$, $W_L W_L$, $Z_L h$, and $W' \rightarrow t\bar{b}$, $W_L Z_L$, $W_L h$. Although the $t\bar{t}$ BR can be large, the KK gluon is degenerate with the electroweak states and have a much larger cross section into the $t\bar{t}$ channel rendering this channel not very useful as a probe of the EW KK's.

LHC signatures: We summarize here the LHC signatures analyzed in Refs. [97, 98]. The total cross section for $pp \rightarrow Z'$ and W' at the LHC with $\sqrt{s} = 14$ TeV are shown in Fig. 8 as a function of its mass. Drell-Yan type production is dominant with vector boson fusion channel about an order of magnitude smaller. We consider next the dominant decay modes, their signatures at the LHC and the reach for their discovery.

Owing to the large mass of the KK Z and W , the SM final states they decay into are significantly boosted resulting in their decay products highly collimated in the lab-frame. For example, for the semi-leptonic $Z' \rightarrow WW$, the presently typical jet reconstruction cone size of $\Delta R = 0.4$ will cause the two jets from the W decay to be reconstructed likely as a single jet (albeit a fat jet), impeding our ability to reconstruct a W mass peak. This means that we would pick up a SM QCD jet background which typically is large, and would require special consideration to keep it from overwhelming the signal. In order to discriminate the merged jets of the W from a QCD jet, one can use the jet-mass, which is the combined invariant mass of the vector sum of 4-momenta of all hadrons making up the jet, as shown in Fig. 9 (left). Techniques to discriminate against QCD jets are also studied in Refs. [100, 101]. Although the two jets from $W \rightarrow jj$ are severely overlapping in the hadronic calorimeter, it may be possible to utilize the better granularity of the electromagnetic calorimeter and the tracker to resolve "sub-jets" [102] and obtain a reasonable discriminating power against QCD. Similarly, in the $W' \rightarrow t\bar{b}$

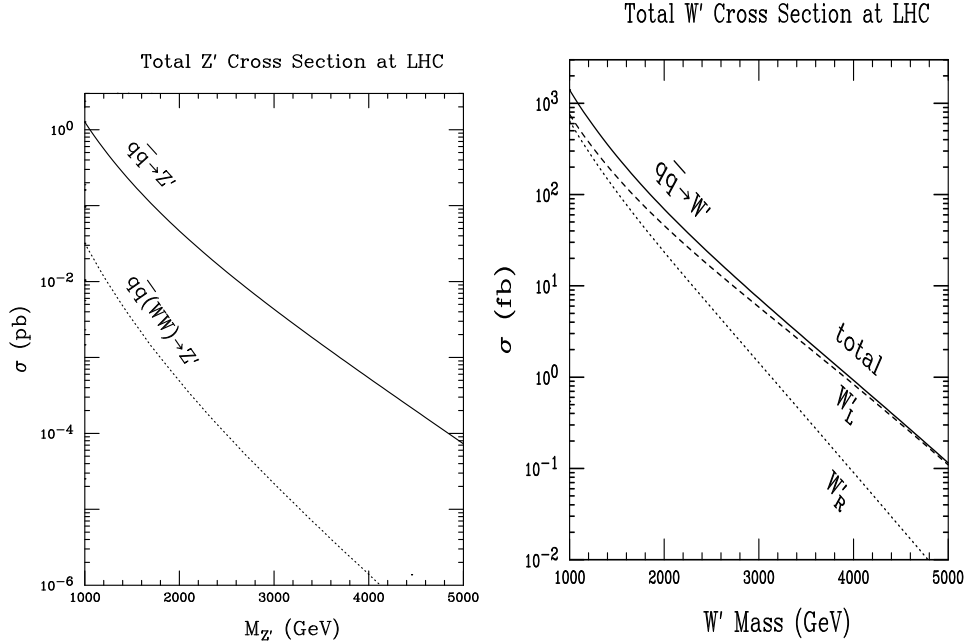


Figure 8. Total cross section for Z' (left) and W' (right) production versus its mass (from Refs. [97] and [98] respectively).

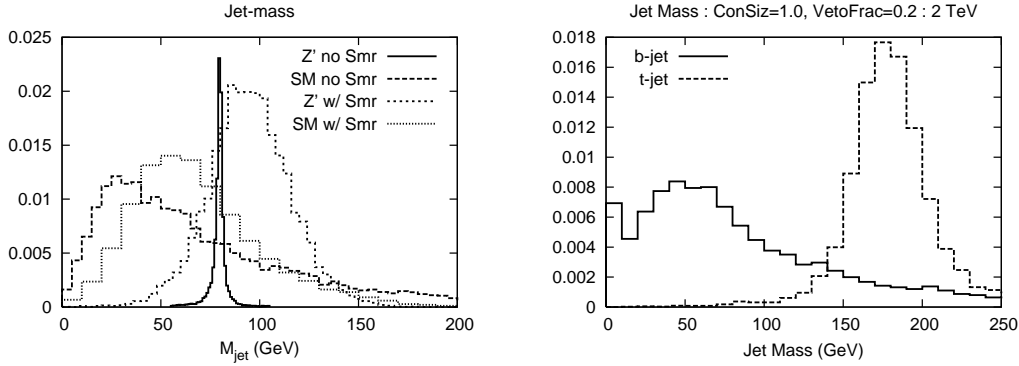


Figure 9. Jet-mass distributions for the $W \rightarrow jj$ vs. QCD jet for a cone-size of 0.4 with and without E , η and ϕ smearing (left), and for t vs. b -jet for a cone-size of 1.0 (right). Both are for a 2 TeV KK gauge boson.

channel, $t\bar{t}$ production can become a source of background since a highly collimated top can fake a b -jet. A top and a b -jet can again be discriminated against by using the jet-mass variable as shown in Fig. 9 (right).

Kinematic cuts can be applied to maximize the signal and suppress the background. We refer the reader to Refs. [97] and [98] for distributions of various kinematic variables for many of the dominant final-states and cuts based on them. We summarize, in Table 1, the LHC reach after suitable cuts for the Z' and W' found in those studies. Where the number of events is small, Poisson statistics is used to find the significance and the equivalent Gaussian significance is quoted. We see that upwards of 300 fb^{-1} is

Table 1. Summary of the best channels (from Refs. [97, 98]) for the Z' (top-table), and, W' (bottom-table), giving the luminosity and significance for the mass shown. For the $W' \rightarrow tb$ channel the numbers without (and with) the reducible $t\bar{t}$ background are shown.

Z' Channel	$M_{Z'}$ (TeV)	\mathcal{L} (fb^{-1})	$\frac{S}{B}$	Significance (σ)
$WW \rightarrow \ell\nu jj$	3	1000	0.2	4.6
$m_h = 120$: $Zh \rightarrow \ell\ell b\bar{b}$	3	1000	2	5.7
$m_h = 150$: $Zh \rightarrow (jj)(jj)\ell\nu$	3	300	1.2	4.7

W' Channel	$M_{W'}$ (TeV)	\mathcal{L} (fb^{-1})	S/B	Significance (σ)
$tb \rightarrow \ell\nu b\bar{b}$	2	1000	0.4 (0.2)	3.4 (2.5)
$ZW \rightarrow \ell\ell\ell\nu$	3	1000	10	6
$m_h = 120$: $Wh \rightarrow \ell\nu b\bar{b}$	3	300	2.4	6.2
$m_h = 150$: $Wh \rightarrow (jj)\ell\nu(jj)$	3	300	4	8

needed to probe a 3 TeV KK Z or W state.

In what we have discussed so far, owing to the flavor connection, the BR into experimentally clean leptonic channels are quite small (about 10^{-3}) rendering them useless, and one had to work with more complicated final states. However, if warped models are taken as a theory of flavor alone (and not generating the gauge-hierarchy), the UV scale can be lowered to as low as $\mathcal{O}(10^3)$ TeV [17] (a more detailed study of flavor constraints in Ref. [103] finds the minimum UV cutoff to be several 10^3 TeV) instead of the usual Planck-scale. Such “truncated” models result in Z' leptonic BR’s that are big enough to lead to a very good significance at the LHC, in the di-lepton channel [17, 104]. A big leptonic cross section due to Z' exchange is also found in Ref. [105] where a model is presented in which the left-handed light quarks and leptons are peaked toward the IR brane giving much larger light fermion couplings to the Z' . However, this comes at the price of requiring the bulk mass c_L parameters for the three generations to be highly degenerate in order to keep FCNC’s under control.

9. KK fermions

The presence of KK excitations of SM fermions is a generic prediction of warped models with bulk fermions and their discovery would be one of the “smoking gun” signatures. For example, see Ref. [106] for how the KK fermion spectrum correlates with the SM fermion masses. However, Ref. [107] points out that discovering these modes would likely be possible only in a future collider and not at the (even upgraded) LHC. This is due to the small single-production cross section and their large mass, as they are heavier than gauge KK modes which are constrained by precision EW measurements. For a model independent analysis at the Tevatron of heavy vector-like fermions with significant mixings with SM fermions, see Ref. [108].

As explained earlier, in order to obtain custodial protection of $Zb\bar{b}$ coupling, the

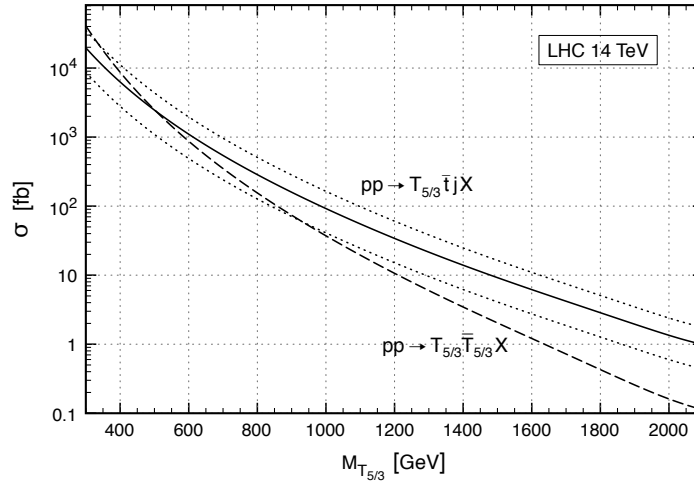


Figure 10. Production cross sections at the LHC for $T_{5/3}$ as a function of its mass. The dashed line refers to pair-production; the solid and the two dotted curves refer to single production for the three values of the coupling. From Ref. [111].

third generation quarks can be extended to be bi-doublets under $SU(2)_L \otimes SU(2)_R$, which then necessitates the introduction of extra non-SM fermions to complete the representation. The presence of these non-SM fermions is model-dependent, but some of them could be fairly light (100's of GeV) [16, 109]. Several works have considered the discovery of these light non-SM fermions at the LHC. In models with custodial protection of $Zb\bar{b}$, the t_R could be in either a singlet of $SU(2)_L \otimes SU(2)_R$ or be in $(1, 3) \oplus (3, 1)$. In the latter case, one of the custodial partners of the t_R , denoted \tilde{b}_R can be fairly light, and Ref. [110] considers its LHC signatures by looking at 4- W events. With 10 fb^{-1} , they show that the peak in the di-jet mass distribution stands out above the background. Ref. [111] considers the single and pair-production of the custodial partner $T_{5/3}$ (of the SM left-handed quark doublet) at the LHC. In Fig. 10 we show from Ref. [111] the cross-sections as a function of its mass. They show that in the *same-sign* di-lepton channel, discovery at the LHC could come with less than 100 pb^{-1} (20 fb^{-1}) of integrated luminosity for a mass of 500 GeV (1 TeV).

Ref. [112] includes the effects of mixings between SM fermions with KK excited fermions and mixings in the gauge sector, and shows that this leads to a better fit to EW observables compared to the SM, including explaining the discrepancy in A_{FB}^b . The effects from fermion mixing in A_{FB}^b is in addition to the contribution from the KK gluon already discussed in Sec. 7. They find, in this class of models, that quite large values of the Higgs mass (about 500 GeV) still give acceptable EW fits.

10. The Radion

The radion is a scalar field associated with fluctuations in the size of the extra dimension. The mass of the radion is dependent on the mechanism that stabilizes the size of the

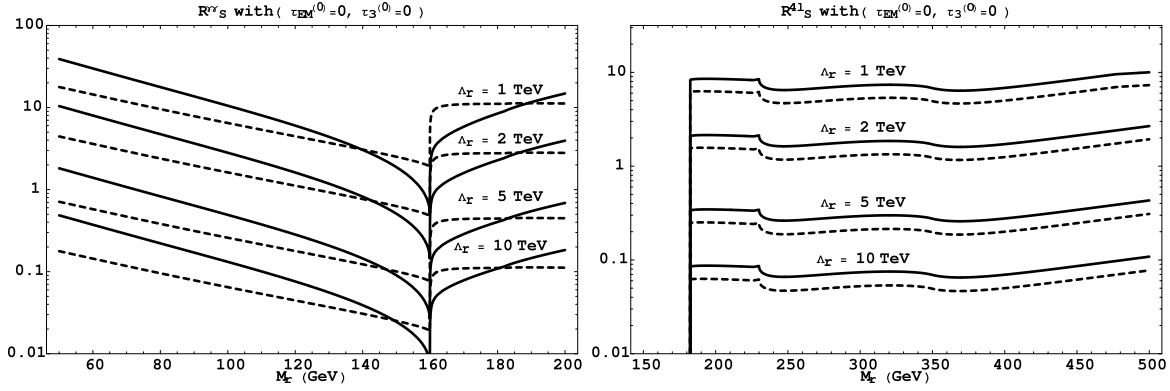


Figure 11. The ratio of the radion significance to the SM Higgs significance in the $\gamma\gamma$ (left) and $ZZ \rightarrow 4\ell$ (right) channels at the LHC. The solid lines are for the case of the SM fields in the bulk, while the dashed are for IR localized SM fields. From Ref. [121].

extra dimension. This was first achieved in a simple model [2] where it can be shown that, generically, the radion may be expected to be the lightest new state in an RS-type setup [113]. This stabilization mechanism was further elaborated in Refs. [114, 115]; for an alternative mechanism based on Casimir energy associated with a compact dimension see, for example, Ref. [116] (an earlier attempt can be found in Ref. [117]). The radion interactions with SM fields, being of 5D gravitational nature, arise through operators of dimension-5 and higher characterized by a scale $\Lambda \sim \text{TeV}$ [113]. For the most part, the radion couplings are similar to Higgs couplings. The radion mass is expected to be a few tens to hundreds of GeV to have escaped detection at LEP and be consistent with precision electroweak data [115, 118]. However, the radion field can mix with the Higgs boson after EWSB which involves another parameter, the coefficient of the curvature-scalar term [119].

LHC signatures of the radion (r) have been analyzed both in the case when SM fields are IR localized (original RS model), as well as when the SM is in the bulk, and the search methodology usually parallels Higgs searches. Similar to the Higgs, the main production channel is $gg \rightarrow r$, induced at loop level in the original RS model, given for example in Ref. [119]. They find that the ratio of the radion significance (in $gg \rightarrow r$ followed by $r \rightarrow \gamma\gamma$ and $r \rightarrow ZZ \rightarrow 4\ell$) to the corresponding SM Higgs significance (R_S) at the LHC can vary from about ten to a hundredth as Λ varies from 500 GeV to 20 TeV (for the coefficient of the curvature-scalar term set to zero).

For the case of the SM in the bulk there is a tree-level coupling of the radion to massless gauge bosons (including the gluon) as pointed out in Ref. [120], and the radion couplings to all SM fields including loop induced couplings can be found in Ref. [121]. R_S from Ref. [121] is shown in Fig. 11 and its variation is similar to that of the original RS case. Here, the curvature-scalar term is assumed to be zero. The $\gamma\gamma$ channel (left) and $ZZ \rightarrow 4\ell$ (right) are shown both for the SM in the bulk (solid lines) and SM fields

IR localized (dashed lines). The dependence on Λ is also shown. Ref. [122] shows that the radion BR into $\gamma\gamma$ can be quite dramatically enhanced in the bulk SM case for non-zero curvature-scalar coupling.

Ref. [123] explores an FCNC observable mediated by the radion $r \rightarrow tc$ at the LHC and finds that an interesting region of parameter space can be probed with 300 fb^{-1} . For a related process, Ref. [65] has shown that the Higgs FCNC $BR(h \rightarrow tc)$ can be about 5×10^{-3} in warped models. They also find that $BR(t \rightarrow hc)$ can be about 10^{-4} . These effects can be looked for at the LHC.

11. Conclusions

We began this review with a detailed presentation of various techniques that are useful in analyzing the physics of theories with extra dimensions, in particular warped extra dimensions. These are the KK description (useful for discussing the collider phenomenology) and techniques that allow to resum the low-energy effects of the new physics (propagator and holographic methods), as well as their relations. An important application is to the determination of indirect bounds on the scale of new physics from EW precision constraints. Models with bulk gauge and fermion fields (that allow addressing the flavour puzzle) together with a custodial symmetry, can be consistent with precision measurements with gauge KK excitation around 3 TeV. Additional flavour constraints (not reviewed here) can result in stronger bounds, although these can be consistent with the above KK scale with a moderate amount of fine-tuning, or with additional flavour structure.

In surveying the collider phenomenology of warped 5D models, we largely focused on their KK signals, both in the original RS model (with the SM content on the IR-brane) and in models that can explain the flavor puzzle within a 5D version of the SM. In these latter models, suppressed couplings to the SM zero modes make the collider discovery of the warped resonances significantly more difficult. In the simplest models, the KK gluons have the best prospects for discovery, up to masses of about 4 TeV, but the KK gravitons, a distinct feature of warped models, would likely lie outside the reach of the LHC experiments. Hence, the upcoming LHC experiments can probe interesting regions of parameters in realistic warped hierarchy/flavor models. Improved analysis techniques, such as those relevant to the hadronic decays of heavy boosted particles, can generally enhance the discovery prospects for the warped KK modes.

Acknowledgments: J. S. would like to acknowledge useful discussions with M. Aybat, R. Contino and especially M. Pérez-Victoria. H. D. and S. G. thank F. Paige for helpful conversations. H. D. and S. G. are supported by the DOE grant DE-AC02-98CH10886. E.P. is supported by DOE under contract DE-FG02-92ER-40699. J.S. is supported by the SNSF under contract 200021-117873.

Appendix A. Low-energy expansions

We collect here some useful results for the functions involved in the calculation of EWPT in models in AdS_5 . We will always consider $L_0 \ll L_1$ and expand to leading order in L_0/L_1 . We also define the dimensionless parameter $\hat{m} \equiv mL_0$, (where m is the mass appearing in the IR boundary conditions).

The function $K_m(p, z)$ defined by Eqs. (25) and (26), which corresponds to the gauge boson holographic profile, is explicitly given by

$$K_m(p, z) = a(z)^{-1} \frac{J_1^z + B Y_1^z}{J_1^0 + B Y_1^0}, \quad (\text{A.1})$$

where $B = -\tilde{J}_1^{\text{IR}}/\tilde{Y}_1^{\text{IR}}$, and we used the definitions of the Bessel functions, Eqs. (5) and (12), but with $m_n \rightarrow p$. The vacuum polarization for the boundary field in the holographic method is

$$K'_m(p, L_0) = -\frac{L_0 \hat{m}}{L_1^2} \left[1 - \frac{\hat{m}}{2}\right] + p^2 L_0 \left[\log \frac{L_1}{L_0} - \frac{\hat{m}}{2}\right] + \frac{p^4 L_0 L_1^2}{2} \left[1 - \frac{5}{8} \hat{m}\right] + \dots \quad (\text{A.2})$$

For an IR localized Higgs, it is sufficient to consider the bulk profile for $z \gg L_0$. Expanding for small momenta and small \hat{m} one finds

$$\begin{aligned} K_m(p, z) = 1 - \frac{z^2}{2L_1^2} \hat{m} \left(1 - \frac{\hat{m}}{2}\right) + p^2 \frac{z^2}{4} \left[1 + 2 \log \frac{L_1}{z} + \hat{m} \left(\frac{z^2}{4L_1^2} - 1\right)\right] \\ + \frac{p^4 z^2 L_1^2}{2 \cdot 32} \left[8 - \frac{z^2}{L_1^2} \left(5 + 4 \log \frac{L_1}{z}\right) + \hat{m} \left(-5 + 2 \frac{z^2}{L_1^2} - \frac{z^4}{6L_1^4}\right)\right] + \dots \end{aligned} \quad (\text{A.3})$$

Similarly, the function $S(p, z)$ defined by Eqs. (25) and (27), which is independent of \hat{m} , is explicitly given by

$$S(p, z) = -\frac{\pi z}{2} (Y_1^0 J_1^z - J_1^0 Y_1^z), \quad (\text{A.4})$$

again with $m_n \rightarrow p$ in the definitions (5). It can be expanded for small p as

$$S(p, z) = \frac{L_0}{2} \left(\frac{z^2}{L_0^2} - 1\right) + p^2 L_0^3 \left[\frac{1}{16} \left(1 - \frac{z^4}{L_0^2}\right) + \frac{z^2}{4L_0^2} \log \frac{z}{L_0}\right] + \dots \quad (\text{A.5})$$

For completeness, we also record the fermion holographic profile [see Eqs. (40) and (41)]:

$$f_L(p, z) = a(z)^{-5/2} \frac{J_{c+1/2}^z + B_f Y_{c+1/2}^z}{J_{c+1/2}^0 + B_f Y_{c+1/2}^0}, \quad (\text{A.6})$$

where $B_f = -\tilde{J}_{c+1/2}^{\text{IR}}/\tilde{Y}_{c+1/2}^{\text{IR}}$, and $m_n \rightarrow p$ in the definitions (5) and (12). The comments about IR localized terms made after Eq. (17) apply. The RH profile can be obtained from $p f_R(p, z) = O_c f_L(p, z)$, where O_c was defined in Eq. (16).

Finally, we also used in the main text the auxiliary functions

$$\begin{aligned} g_n(c) &\equiv \int_{L_0}^{L_1} dz \left(\frac{z}{L_1}\right)^n a(z)^4 [f_L^0(z)]^2 \\ &= \left(\frac{L_0}{L_1}\right)^n \frac{2c-1}{2c-n-1} \frac{1 - \left(\frac{L_0}{L_1}\right)^{2c-n-1}}{1 - \left(\frac{L_0}{L_1}\right)^{2c-1}}, \end{aligned} \quad (\text{A.7})$$

$$\begin{aligned}
\tilde{g}_n(c) &\equiv \int_{L_0}^{L_1} dz \log\left(\frac{z}{L_1}\right) \left(\frac{z}{L_1}\right)^n a(z)^4 [f_L^0(z)]^2 \\
&= \left(\frac{L_0}{L_1}\right)^n \frac{2c-1}{(2c-n-1)^2} \frac{1 - (2c-n-1) \log \frac{L_1}{L_0} - \left(\frac{L_0}{L_1}\right)^{2c-n-1}}{1 - \left(\frac{L_0}{L_1}\right)^{2c-1}}. \quad (\text{A.8})
\end{aligned}$$

Note that as $c \rightarrow +\infty$, $g_n(c) \rightarrow (L_0/L_1)^n$ and $\tilde{g}_n(c) \rightarrow (L_0/L_1)^n \ln L_0/L_1$, which are exponentially small for positive n . Expanding the functions of Eq. (102) for small p^2 using Eq. (A.3), one gets

$$\bar{g}_i(p^2) = \bar{g}_i(0) + p^2 \bar{g}'_i(0) + \frac{1}{2} p^4 \bar{g}''_i(0) + \dots, \quad (\text{A.9})$$

where

$$\bar{g}_i(0) = 1 - \frac{1}{2} \hat{m} \left(1 - \frac{1}{2} \hat{m}\right) g_2, \quad (\text{A.10})$$

$$\bar{g}'_i(0) = \frac{L_1^2}{4} \left[g_2 - 2\tilde{g}_2 + \hat{m} \left(\frac{1}{4} g_4 - g_2 \right) \right], \quad (\text{A.11})$$

$$\bar{g}''_i(0) = \frac{L_1^4}{32} \left[8g_2 - 5g_4 + 4\tilde{g}_4 + \hat{m} \left(-5g_2 + 2g_4 - \frac{1}{6} g_6 \right) \right], \quad (\text{A.12})$$

and \hat{m} corresponds to \hat{m} , 0 and \hat{m}/c^2 for $f = W, V, A$, respectively.

References

- [1] L. Randall and R. Sundrum, Phys. Rev. Lett. **83**, 3370 (1999) [arXiv:hep-ph/9905221].
- [2] W. D. Goldberger and M. B. Wise, Phys. Rev. Lett. **83**, 4922 (1999) [arXiv:hep-ph/9907447].
- [3] H. Davoudiasl, J. L. Hewett and T. G. Rizzo, Phys. Rev. Lett. **84**, 2080 (2000) [arXiv:hep-ph/9909255].
- [4] W. D. Goldberger and M. B. Wise, Phys. Rev. D **60**, 107505 (1999) [arXiv:hep-ph/9907218].
- [5] H. Davoudiasl, J. L. Hewett and T. G. Rizzo, Phys. Lett. B **473**, 43 (2000) [arXiv:hep-ph/9911262].
- [6] A. Pomarol, Phys. Lett. B **486**, 153 (2000) [arXiv:hep-ph/9911294].
- [7] Y. Grossman and M. Neubert, Phys. Lett. B **474**, 361 (2000) [arXiv:hep-ph/9912408].
- [8] T. Gherghetta and A. Pomarol, Nucl. Phys. B **586**, 141 (2000) [arXiv:hep-ph/0003129].
- [9] M. S. Carena, E. Pontón, J. Santiago and C. E. M. Wagner, Phys. Rev. D **76**, 035006 (2007) [arXiv:hep-ph/0701055].
- [10] S. J. Huber and Q. Shafi, Phys. Lett. B **498**, 256 (2001) [arXiv:hep-ph/0010195]; S. J. Huber, Nucl. Phys. B **666**, 269 (2003) [arXiv:hep-ph/0303183].
- [11] G. Burdman, Phys. Rev. D **66**, 076003 (2002) [arXiv:hep-ph/0205329]; Phys. Lett. B **590**, 86 (2004) [arXiv:hep-ph/0310144].
- [12] K. Agashe, G. Perez and A. Soni, Phys. Rev. Lett. **93**, 201804 (2004) [arXiv:hep-ph/0406101].
- [13] K. Agashe, G. Perez and A. Soni, Phys. Rev. D **71**, 016002 (2005) [arXiv:hep-ph/0408134].
- [14] K. Agashe, A. E. Blechman and F. Petriello, Phys. Rev. D **74**, 053011 (2006) [arXiv:hep-ph/0606021].
- [15] K. Agashe, A. Delgado, M. J. May and R. Sundrum, JHEP **0308**, 050 (2003) [arXiv:hep-ph/0308036].
- [16] K. Agashe, R. Contino, L. Da Rold and A. Pomarol, Phys. Lett. B **641**, 62 (2006) [arXiv:hep-ph/0605341].
- [17] H. Davoudiasl, G. Perez and A. Soni, Phys. Lett. B **665**, 67 (2008) [arXiv:0802.0203 [hep-ph]].
- [18] L. Randall and M. D. Schwartz, JHEP **0111**, 003 (2001) [arXiv:hep-th/0108114].
- [19] C. Csaki, C. Grojean, H. Murayama, L. Pilo and J. Terning, Phys. Rev. D **69**, 055006 (2004) [arXiv:hep-ph/0305237].

- [20] H. Davoudiasl, J. L. Hewett and T. G. Rizzo, Phys. Rev. D **68**, 045002 (2003) [arXiv:hep-ph/0212279].
- [21] M. S. Carena, E. Pontón, T. M. P. Tait and C. E. M. Wagner, Phys. Rev. D **67** (2003) 096006 [arXiv:hep-ph/0212307]; M. S. Carena, A. Delgado, E. Pontón, T. M. P. Tait and C. E. M. Wagner, Phys. Rev. D **68**, 035010 (2003) [arXiv:hep-ph/0305188].
- [22] N. S. Manton, Nucl. Phys. B **158**, 141 (1979).
- [23] Y. Hosotani, Phys. Lett. B **126**, 309 (1983).
- [24] N. V. Krasnikov, Phys. Lett. B **273**, 246 (1991).
- [25] H. Hatanaka, T. Inami and C. S. Lim, Mod. Phys. Lett. A **13**, 2601 (1998) [arXiv:hep-th/9805067].
- [26] R. Contino, Y. Nomura and A. Pomarol, Nucl. Phys. B **671**, 148 (2003) [arXiv:hep-ph/0306259].
- [27] K. Agashe, R. Contino and A. Pomarol, Nucl. Phys. B **719**, 165 (2005) [arXiv:hep-ph/0412089].
- [28] H. Davoudiasl, J. L. Hewett and T. G. Rizzo, JHEP **0308** (2003) 034 [arXiv:hep-ph/0305086].
- [29] N. Arkani-Hamed, L. J. Hall, Y. Nomura, D. Tucker-Smith and N. Weiner, Nucl. Phys. B **605**, 81 (2001) [arXiv:hep-ph/0102090].
- [30] A. Falkowski and M. Perez-Victoria, arXiv:0810.4940 [hep-ph].
- [31] F. del Aguila, M. Perez-Victoria and J. Santiago, JHEP **0302**, 051 (2003) [arXiv:hep-th/0302023].
- [32] M. S. Carena, A. Delgado, E. Pontón, T. M. P. Tait and C. E. M. Wagner, Phys. Rev. D **71**, 015010 (2005) [arXiv:hep-ph/0410344].
- [33] R. Contino and A. Pomarol, JHEP **0411**, 058 (2004) [arXiv:hep-th/0406257].
- [34] W. Buchmuller and D. Wyler, Nucl. Phys. B **268**, 621 (1986).
- [35] F. del Aguila, M. Perez-Victoria and J. Santiago, Phys. Lett. B **492** (2000) 98 [arXiv:hep-ph/0007160]; JHEP **0009** (2000) 011 [arXiv:hep-ph/0007316].
- [36] F. del Aguila and J. Santiago, Phys. Lett. B **493** (2000) 175 [arXiv:hep-ph/0008143]; JHEP **0203** (2002) 010 [arXiv:hep-ph/0111047].
- [37] R. Barbieri, A. Pomarol, R. Rattazzi and A. Strumia, Nucl. Phys. B **703**, 127 (2004) [arXiv:hep-ph/0405040].
- [38] T. Gherghetta, arXiv:hep-ph/0601213.
- [39] C. Amsler *et al.* [Particle Data Group], Phys. Lett. B **667**, 1 (2008).
- [40] Z. Han and W. Skiba, Phys. Rev. D **71** (2005) 075009 [arXiv:hep-ph/0412166]; Z. Han, Phys. Rev. D **73**, 015005 (2006) [arXiv:hep-ph/0510125].
- [41] G. Cacciapaglia, C. Csaki, G. Marandella and A. Strumia, Phys. Rev. D **74**, 033011 (2006) [arXiv:hep-ph/0604111].
- [42] C. Csaki, J. Erlich and J. Terning, Phys. Rev. D **66**, 064021 (2002) [arXiv:hep-ph/0203034].
- [43] M. E. Peskin and T. Takeuchi, Phys. Rev. Lett. **65**, 964 (1990); Phys. Rev. D **46**, 381 (1992).
- [44] Z. Chacko, M. A. Luty and E. Pontón, JHEP **0007**, 036 (2000) [arXiv:hep-ph/9909248].
- [45] M. S. Carena, E. Pontón, J. Santiago and C. E. M. Wagner, Nucl. Phys. B **759**, 202 (2006) [arXiv:hep-ph/0607106].
- [46] K. Agashe and R. Contino, Nucl. Phys. B **742** (2006) 59 [arXiv:hep-ph/0510164].
- [47] [Tevatron Electroweak Working Group and CDF Collaboration and D0 Collab], arXiv:0903.2503 [hep-ex].
- [48] [CDF Collaboration and D0 Collaboration], arXiv:0808.0147 [hep-ex].
- [49] A. Falkowski and M. Perez-Victoria, JHEP **0812** (2008) 107 [0806.1737 [hep-ph]];
- [50] B. Batell, T. Gherghetta and D. Sword, Phys. Rev. D **78** (2008) 116011 [0808.3977 [hep-ph]];
- [51] A. Delgado and D. Diego, 0905.1095 [hep-ph].
- [52] S. M. Aybat and J. Santiago, arXiv:0905.3032 [hep-ph].
- [53] T. Gherghetta and D. Sword, arXiv:0907.3523 [hep-ph].
- [54] G. Cacciapaglia, C. Csaki, C. Grojean and J. Terning, Phys. Rev. D **71**, 035015 (2005) [arXiv:hep-ph/0409126].
- [55] G. Cacciapaglia, C. Csaki, G. Marandella and J. Terning, Phys. Rev. D **75**, 015003 (2007) [arXiv:hep-ph/0607146].
- [56] C. Grojean, Comptes Rendus Physique **8**, 1068 (2007).

- [57] C. Csaki, J. Hubisz and P. Meade, arXiv:hep-ph/0510275.
- [58] C. Csaki, A. Falkowski and A. Weiler, JHEP **0809**, 008 (2008) [arXiv:0804.1954 [hep-ph]].
- [59] S. Casagrande, F. Goertz, U. Haisch, M. Neubert and T. Pfoh, JHEP **0810**, 094 (2008) [arXiv:0807.4937 [hep-ph]].
- [60] M. Blanke, A. J. Buras, B. Duling, S. Gori and A. Weiler, JHEP **0903** (2009) 001 [arXiv:0809.1073 [hep-ph]].
- [61] K. Agashe, A. Azatov and L. Zhu, Phys. Rev. D **79** (2009) 056006 [arXiv:0810.1016 [hep-ph]].
- [62] M. Blanke, A. J. Buras, B. Duling, K. Gemmler and S. Gori, JHEP **0903** (2009) 108 [arXiv:0812.3803 [hep-ph]].
- [63] M. E. Albrecht, M. Blanke, A. J. Buras, B. Duling and K. Gemmler, arXiv:0903.2415 [hep-ph].
- [64] O. Gedalia, G. Isidori and G. Perez, arXiv:0905.3264 [hep-ph].
- [65] K. Agashe and R. Contino, arXiv:0906.1542 [hep-ph].
- [66] A. Azatov, M. Toharia and L. Zhu, arXiv:0906.1990 [hep-ph].
- [67] G. Cacciapaglia, C. Csaki, J. Galloway, G. Marandella, J. Terning and A. Weiler, JHEP **0804**, 006 (2008) [arXiv:0709.1714 [hep-ph]].
- [68] A. L. Fitzpatrick, G. Perez and L. Randall, arXiv:0710.1869 [hep-ph].
- [69] C. Cheung, A. L. Fitzpatrick and L. Randall, JHEP **0801**, 069 (2008) [arXiv:0711.4421 [hep-th]].
- [70] A. L. Fitzpatrick, L. Randall and G. Perez, Phys. Rev. Lett. **100**, 171604 (2008).
- [71] J. Santiago, JHEP **0812**, 046 (2008) [arXiv:0806.1230 [hep-ph]].
- [72] C. Csaki, A. Falkowski and A. Weiler, Phys. Rev. D **80**, 016001 (2009) [arXiv:0806.3757 [hep-ph]].
- [73] K. Agashe, arXiv:0902.2400 [hep-ph].
- [74] C. Csaki, G. Perez, Z. Surujon and A. Weiler, arXiv:0907.0474 [hep-ph].
- [75] M. C. Chen, K. T. Mahanthappa and F. Yu, arXiv:0907.3963 [hep-ph].
- [76] T. Aaltonen *et al.* [CDF Collaboration], Phys. Rev. Lett. **102**, 091805 (2009) [arXiv:0811.0053 [hep-ex]].
- [77] V. M. Abazov *et al.* [D0 Collaboration], Phys. Rev. Lett. **100**, 091802 (2008) [arXiv:0710.3338 [hep-ex]].
- [78] K. Agashe, H. Davoudiasl, G. Perez and A. Soni, Phys. Rev. D **76**, 036006 (2007) [arXiv:hep-ph/0701186].
- [79] B. C. Allanach, K. Odagiri, M. J. Palmer, M. A. Parker, A. Sabetfakhri and B. R. Webber, JHEP **0212**, 039 (2002) [arXiv:hep-ph/0211205].
- [80] I. Belotelov *et al.*, CERN-CMS-NOTE-2006-104.
- [81] H. Davoudiasl, J. L. Hewett and T. G. Rizzo, Phys. Rev. D **63**, 075004 (2001) [arXiv:hep-ph/0006041].
- [82] A. L. Fitzpatrick, J. Kaplan, L. Randall and L. T. Wang, arXiv:hep-ph/0701150.
- [83] J.E. Huth *et al.*, *Proceedings of Research Directions For The Decade: Snowmass Accord 1990*.
- [84] O. Antipin, D. Atwood and A. Soni, Phys. Lett. B **666**, 155 (2008) [arXiv:0711.3175 [hep-ph]].
- [85] O. Antipin and A. Soni, JHEP **0810**, 018 (2008) [arXiv:0806.3427 [hep-ph]].
- [86] H. Murayama and V. Rentala, arXiv:0904.4561 [hep-ph].
- [87] F. Gianotti *et al.*, Eur. Phys. J. C **39**, 293 (2005) [arXiv:hep-ph/0204087].
- [88] O. Bruning *et al.*, CERN-LHC-PROJECT-REPORT-626
- [89] K. Agashe, A. Belyaev, T. Krupovnickas, G. Perez and J. Virzi, arXiv:hep-ph/0612015.
- [90] B. Lillie, L. Randall and L. T. Wang, arXiv:hep-ph/0701166.
- [91] B. Lillie, L. Randall and L. T. Wang, JHEP **0709**, 074 (2007) [arXiv:hep-ph/0701166]. V. Barger, T. Han and D. G. E. Walker, Phys. Rev. Lett. **100**, 031801 (2008) [arXiv:hep-ph/0612016]; U. Baur and L. H. Orr, Phys. Rev. D **76**, 094012 (2007) [arXiv:0707.2066 [hep-ph]] and Phys. Rev. D **77**, 114001 (2008) [arXiv:0803.1160 [hep-ph]]; Y. Bai and Z. Han, arXiv:0809.4487 [hep-ph].
- [92] J. Thaler and L. T. Wang, JHEP **0807**, 092 (2008) [arXiv:0806.0023 [hep-ph]]; D. E. Kaplan, K. Rehermann, M. D. Schwartz and B. Tweedie, arXiv:0806.0848 [hep-ph]; L. G. Almeida, S. J. Lee, G. Perez, I. Sung and J. Virzi, arXiv:0810.0934 [hep-ph].

- [93] A. Djouadi, G. Moreau and R. K. Singh, Nucl. Phys. B **797**, 1 (2008) [arXiv:0706.4191 [hep-ph]].
- [94] A. Djouadi, G. Moreau, F. Richard and R. K. Singh, arXiv:0906.0604 [hep-ph].
- [95] A. Djouadi, G. Moreau and F. Richard, Nucl. Phys. B **773**, 43 (2007) [arXiv:hep-ph/0610173].
- [96] M. Guchait, F. Mahmoudi and K. Sridhar, Phys. Lett. B **666**, 347 (2008) [arXiv:0710.2234 [hep-ph]].
- [97] K. Agashe *et al.*, Phys. Rev. D **76**, 115015 (2007) [arXiv:0709.0007 [hep-ph]].
- [98] K. Agashe, S. Gopalakrishna, T. Han, G. Y. Huang and A. Soni, arXiv:0810.1497 [hep-ph].
- [99] M. Piai, arXiv:0704.2205 [hep-ph].
- [100] D. Bencheekroun, C. Driouichi, A. Hoummada, SN-ATLAS-2001-001, ATL-COM-PHYS-2000-020, EPJ Direct 3, 1 (2001); W. Skiba and D. Tucker-Smith, Phys. Rev. D **75**, 115010 (2007) [arXiv:hep-ph/0701247]; See also talk by Gustaaf Brooijmans at the "Workshop on Possible Parity Restoration at High Energy", Beijing (China) June 11-12, 2007.
- [101] L. G. Almeida, S. J. Lee, G. Perez, G. Sterman, I. Sung and J. Virzi, arXiv:0807.0234 [hep-ph].
- [102] M. Strassler, "Unusual Physics Signatures at the LHC," talk presented at the 2007 Phenomenology Symposium - Pheno 07, University of Wisconsin, Madison, May 7-9, 2007; Frank Paige, private communication; The ATLAS Collaboration, ATL-PHYS-PUB-2009-081, ATL-COM-PHYS-2009-255; The CMS Collaboration CMS PAS JME-09-001, CMS PAS EXO-09-002.
- [103] M. Bauer, S. Casagrande, L. Grunder, U. Haisch and M. Neubert, arXiv:0811.3678 [hep-ph].
- [104] H. Davoudiasl, S. Gopalakrishna and A. Soni, arXiv:0908.1131 [hep-ph].
- [105] F. Ledroit, G. Moreau and J. Morel, JHEP **0709**, 071 (2007) [arXiv:hep-ph/0703262].
- [106] H. Davoudiasl and A. Soni, Phys. Rev. D **76**, 095015 (2007) [arXiv:0705.0151 [hep-ph]].
- [107] H. Davoudiasl, T. G. Rizzo and A. Soni, Phys. Rev. D **77**, 036001 (2008) [arXiv:0710.2078 [hep-ph]].
- [108] A. Atre, M. Carena, T. Han and J. Santiago, arXiv:0806.3966 [hep-ph].
- [109] K. Agashe and G. Servant, Phys. Rev. Lett. **93**, 231805 (2004) [arXiv:hep-ph/0403143]; JCAP **0502**, 002 (2005) [arXiv:hep-ph/0411254].
- [110] C. Dennis, M. Karagoz Unel, G. Servant and J. Tseng, arXiv:hep-ph/0701158.
- [111] R. Contino and G. Servant, JHEP **0806**, 026 (2008) [arXiv:0801.1679 [hep-ph]].
- [112] C. Bouchart and G. Moreau, Nucl. Phys. B **810**, 66 (2009) [arXiv:0807.4461 [hep-ph]].
- [113] W. D. Goldberger and M. B. Wise, Phys. Lett. B **475**, 275 (2000) [arXiv:hep-ph/9911457].
- [114] O. DeWolfe, D. Z. Freedman, S. S. Gubser and A. Karch, Phys. Rev. D **62**, 046008 (2000) [arXiv:hep-th/9909134].
- [115] C. Csaki, M. L. Graesser and G. D. Kribs, Phys. Rev. D **63**, 065002 (2001) [arXiv:hep-th/0008151].
- [116] J. Garriga and A. Pomarol, Phys. Lett. B **560**, 91 (2003) [arXiv:hep-th/0212227].
- [117] W. D. Goldberger and I. Z. Rothstein, Phys. Lett. B **491**, 339 (2000) [arXiv:hep-th/0007065].
- [118] J. F. Gunion, M. Toharia and J. D. Wells, Phys. Lett. B **585**, 295 (2004) [arXiv:hep-ph/0311219].
- [119] G. F. Giudice, R. Rattazzi and J. D. Wells, Nucl. Phys. B **595**, 250 (2001) [arXiv:hep-ph/0002178].
- [120] T. G. Rizzo, JHEP **0206**, 056 (2002) [arXiv:hep-ph/0205242].
- [121] C. Csaki, J. Hubisz and S. J. Lee, Phys. Rev. D **76**, 125015 (2007) [arXiv:0705.3844 [hep-ph]].
- [122] M. Toharia, Phys. Rev. D **79**, 015009 (2009) [arXiv:0809.5245 [hep-ph]].
- [123] A. Azatov, M. Toharia and L. Zhu, arXiv:0812.2489 [hep-ph].